

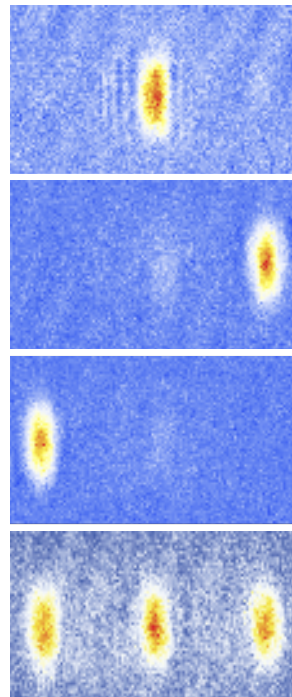
BRAGG SCATTERING OF A RELEASED BOSE-EINSTEIN CONDENSATE ON AN ATOM-CHIP

Author:

Robert Altmann

Supervisor:

Dr. N.J. van Druten



MSc Physics: advanced matter and energy physics

Submitted: July, 2012

University of Amsterdam

Institute of physics

Van der Waals-Zeeman institute

Quantum gases and quantum information

Second corrector:

Prof. Dr H.B. van den Linden van den Heuvell

Daily supervisors:

Dr. W. Lewoczko-Adamczyk

Dr. Q. Beaufils

Dr. S. Lepoutre

Abstract

One-dimensional (1D) gases exhibit interesting phenomena that are not present in either 2D or 3D. Atom chips offer an attractive route to creating and manipulating such 1D gases. By employing specifically designed wire patterns, the magnetic trapping potential of our chip features a strong harmonic confinement in the radial direction. For this project we aimed to build an experimental setup to enhance this atom-chip experiment with an optical lattice in the axial direction. An experimental way to determine if the optical lattice perturbs the atoms is to do Bragg diffraction experiments. This thesis presents the theoretical framework that describes Bragg scattering of a released Bose-Einstein condensate, the building of the experimental setup and the obtained results.

With our setup we observed Rabi-oscillations, the resonance spectrum and the momentum selectivity which are characteristics of Bragg scattering. Finally we also showed that by adjusting the parameters of our optical lattice that we can enter a different diffraction regimen, that of Raman-Nath. From this we conclude that we have build an optical lattice that can be used to do experiments on one-dimensional Bose-Einstein condensates on an atom chip.

Contents

Abstract	3
Chapter 1. Introduction	7
Chapter 2. Theoretical background	9
2.1. Atom interaction with light	10
2.1.1. Introducing a two level system	10
2.1.2. Perturbation by an oscillating electric field	10
2.2. Density matrix formalism for the two level system	13
2.2.1. Basic concepts	13
2.2.2. Two level system and the density matrix approach	15
2.2.3. Spontaneous emission	17
2.3. Laser cooling and trapping	18
2.3.1. Scattering force	18
2.3.2. Optical molasses	20
2.3.3. The magneto-optical trap	23
2.4. The dipole force	24
2.4.1. Dipole interaction with the light field	25
2.4.2. Focused beam traps	28
2.4.3. 1D lattice potential	29
2.5. Magnetic trapping and evaporative cooling	29
2.5.1. Magnetic trapping	29
2.5.2. Evaporative cooling	30
2.5.3. Bose-Einstein condensation	30
2.6. Bragg scattering of cold atoms	31
2.6.1. 2-photon scattering process	32
2.6.2. Rabi oscillations in momentum space	34
Chapter 3. The experimental setup	36
3.1. The Celsius experiment	36
3.1.1. Atom-chip experiments	36
3.1.2. The Celsius experiment	38
3.2. Bragg lasers	40
3.2.1. Laser setup	41
3.2.2. Expected results	46
Chapter 4. Results	48
4.1. Analyzing data	48
4.2. Rabi oscillations	49
4.3. Bragg-spectrum	51

4.4.	Momentum selectivity	53
4.4.1.	A neat application	54
4.5.	Raman-Nath scattering	54
Chapter 5.	Conclusion & Outlook	58
Appendix A.	Fundamental constants	60
Appendix B.	Saturation intensity	61
Appendix C.	Light shift	62
Appendix D.	Radiative selection rules	64
Appendix E.	Effective Rabi-frequency for first order Bragg scattering	65
Bibliography		68
Nederlandse samenvatting		70
Acknowledgments		72

CHAPTER 1

Introduction

The field of *quantum gases* and *Bose-Einstein condensation* which forms the background of this thesis is a field with many aspects and great variety. In order to realize any successful experiment in this field one has to gain knowledge of a number of techniques and technologies. That this is not a trivial task is reflected in the time took to realize the first Bose-Einstein condensate in a dilute gas. In 1924 the Indian physicist Bose made the first calculations regarding light particles and used a statistical argument to derive the black-body photon spectrum. In this period, however, the idea that light consists of particles was still highly controversial and Bose was unable to publish his work. Only after sending it to Einstein, who realized its importance, the work gained the interest of the scientific community [1]. Einstein extended the work of Bose to atoms and the result was the Bose-Einstein statistics [2]. Based on this new statistics Einstein noticed a peculiar feature in the distribution of atoms over the quantized energy levels. At a very low but finite temperature a large fraction of the atoms would go into the lowest quantum energy state. This process is now known as Bose-Einstein condensation and the condition for this to occur is roughly that the deBroglie wavelength, λ_{dB} , must be larger than the inter particle spacing. Bose and Einstein were the first to bring out the idea that Bose-Einstein condensation would display quantum behavior on a macroscopic scale which was the primary reason for much of the interest in this phenomena [3].

After this prediction scientist have tried to make this exotic state of matter in the laboratory. It took several technological advances such as the invention of the laser cooling, magnetic trapping and evaporative cooling before scientists finally reached this goal in 1995. This has been a major achievement in experimental physics and was awarded with the Nobel prize in 2001 (Cornell, Ketterle and Wiemann). Although this realization was already 17 years ago these systems are still studied intensively in labs all over the world. One of the most fundamental things that can be studied in these systems is the interactions between particles because it is these interactions that lie on the basis of the condensation process. Furthermore it also provides a testing ground for many body phenomena. Many theories have been developed over the years that can now be tested because of the large range of control over the system. It is also interesting from the perspective of different research field such as hard condensed matter. In these systems hard condensed matter systems can be simulated with the advantage that there is a larger range of control and measuring is easier. Besides fundamental research at different levels as motivation for studying Bose-Einstein condensates there are also several applications hypothesized using quantum gases. Some possible applications could be precision sensing and quantum information processing(for a long review of physics that can be done using the wave nature of matter see [4]).

The work for this thesis has been carried out at he University of Amsterdam in the Van der Waals-Zeeman institute in the collective group of quantum gases and quantum information. The van der Waals-Zeeman institute has a rich history in the field of quantum degenerate gases and the particular group where this work was done focuses on low-dimensional condensates on atom chips called the *Celsius* experiment (Chip Experiment for Low-dimensional Strongly Interacting Ultra-cold Systems)[5]. There are several advantages to using atom-chips to do cold atom experiments with respect to the conventional way. Scale reduction an reproducibility make the atom chips extremely useful. Also

experimental cycle time is shortened reducing the demands on for example the vacuum. But the most intriguing feature of the atom chip is the possibility to design elaborate magnetic potentials [6]. In our case that means the possibility to create single one dimensional Bose-Einstein condensates. The motivation for this project was to enhance this atom-chip experiment with an one dimensional optical lattice in the longitudinal direction. With this addition to the experiment interesting features in one dimension could be tested such as the quantum Newtons Cradle [7]. Another possibility would be to study the superfluid to Mott-insulator transition a single one dimensional sample (for reference see [8]). And of course, as a long term goal in the field of quantum gases, condensates in combination with optical lattices have been proposed as possible setups to do quantum information processing [9].

The aim of the project for this thesis was to build the experimental setup for the optical lattice and implement it on the Celsius experiment. The next goal was to characterize the setup and show that the atoms are scattered by the optical lattice potential. In order to achieve this the idea was to do Bragg diffraction experiments. Because this is a resonant process the characteristics are relatively easy to recognize and in this way a good tool for determining the possibilities for further experiments.

This thesis consist of three main chapters. In chapter one the general theory about atom-light interaction and the techniques used to reach Bose-Einstein condensation is reviewed. At the end of the chapter the theory about Bragg diffraction of a condensate is described. Because of the importance of the atom chip in our experiment a description of the basic working and the experimental setup is given in chapter 2. In the second part of this chapter the experimental setup to enhance the chip experiment with an optical lattice is described. The experimental result and the way they were analyzed are reported in chapter 4.

CHAPTER 2

Theoretical background

In this chapter the main theory concerning the cooling and trapping of atoms using laser light and magnetic fields relevant for this thesis is described. To study the basic interaction between light and atoms a toy model is used where an atom is considered that has only two discrete energy levels. This is a great simplification however, for the alkali metals it is not a bad approximation and it is useful as a tool to understand the basic interactions between light and atoms. The interaction of atoms with light can be broken down in two main parts. A dissipative part and a conservative part of interaction. The dissipative part of the interaction is described by an atom absorbing a photon from the light field which has two consequences. The first being that the atom gains internal energy by absorbing the photon and go into an excited state. Then via spontaneous emission of a photon, in a random direction, it can relax back to the ground state or, if the laser field is intense enough, stimulated emission actively causes the atom to go back into the ground state. The absorption of radiation energy causes the atom to undergo Rabi oscillations between the population in the ground and the excited state. This interaction will be described in two different formalisms in section 2.1 and 2.2. The second consequence of an atom absorbing an photon is the transfer of momentum. This photon momentum transfer leads to a velocity dependent force on the atoms. Since the spread of velocities of a gas of atoms is directly related to its temperature we can use this force to slow down the atoms considerably which results in cooling of the atomic sample. This interaction described in section 2.3 and is called *optical molasses*. Although atoms are cooled down in the optical molasses using the force of light, this interaction does not constitute a trap. To be able to study the atoms over longer periods of time an additional feature has to be added to create a trapping potential. In order to create this trap magnetic fields are added to create the so called *magneto-optical trap* (section 2.3.3). Using these techniques atoms can be cooled down to such low temperatures that quantum effects start to play a role. There are however limits to these cooling mechanisms and to cool down atoms even further and to go deeper into the quantum regime different techniques have to be used such as evaporative cooling which is described shortly in section (2.5).

Secondly, there is the conservative component of the atom-light interaction which arises from the interaction of the light field with the induced dipole moment of the atom. The light field causes the energy levels of the atom to shift, called light shift or ac-Stark shift. For light fields with large detunings from atomic resonance spontaneous emission processes can be neglected and the energy shift can be used to create a conservative trapping potential for neutral atoms. In a standing wave this *dipole potential* constitutes an array or lattice of potential wells (section 2.4). Such an periodic potential for neutral atoms is a useful tool for studying properties of quantum mechanics.

The last section of this chapter will be used to discuss one application of the above mentioned techniques called *Bragg scattering*. This is a technique that allows one to coherently manipulate a cold atomic cloud or Bose-Einstein condensate using the interaction of light and atoms. This section will give the theoretical background for the experiments described in chapter 3 and the results in chapter 4.

2.1. Atom interaction with light

In this section absorption of a photon by a two level atom is studied. Starting from the Schrödinger equation we are able to derive a set of rate equations that describe the populations of the atomic energy levels

2.1.1. Introducing a two level system. We study the interaction of an atom with radiation and assume that the atom has only two energy levels as depicted in figure 2.1. To describe this system we use a *semi-classical* approach, i.e. the radiation is treated as a classical field but the atom is described using quantum mechanics. We start from the time dependent Schrödinger equation

$$i\hbar \frac{\partial \Psi}{\partial t} = (H_0 + H_I(t)) \Psi \quad (2.1)$$

where the time-dependent term of the Hamiltonian H_I describes the interaction with the light field that perturbs the eigenfunctions of H_0 . The unperturbed eigenvalues and eigenfunctions of H_0 are just the atomic energy levels as described in any atomic physics text book. We write the wavefunction for an energy level E

$$\Psi_n(\mathbf{r}, t) = \sum_n \psi_n(\mathbf{r}) e^{-iE_n t/\hbar} \quad (2.2)$$

Since the system we are considering has only two energy levels, lets say a ground state and an excited state the spatial wave functions must satisfy

$$H_0 \psi_G(\mathbf{r}) = E_G \psi_G(\mathbf{r}) \quad (2.3)$$

$$H_0 \psi_E(\mathbf{r}) = E_E \psi_E(\mathbf{r}) \quad (2.4)$$

These wave functions are not the stationary states of the full Hamiltonian, $H_0 + H_I(t)$, but we can express the wave function at any time as a function of these spatial wave functions. In Dirac ket notation and using the fact that $\omega_n = E_n/\hbar$ the wavefunction becomes

$$\Psi(\mathbf{r}, t) = c_G(t) |G\rangle e^{-i\omega_G t} + c_E(t) |E\rangle e^{-i\omega_E t} \quad (2.5)$$

Normalization requires that the time dependent coefficients satisfy

$$\langle \Psi | \Psi \rangle = |c_G(t)|^2 + |c_E(t)|^2 = 1 \quad (2.6)$$

2.1.2. Perturbation by an oscillating electric field. Let us now introduce an oscillating electric field

$$\mathbf{E}(\mathbf{r}, t) = \mathbf{E}_0(\mathbf{r}) \cos(\omega t) \quad (2.7)$$

that produces the perturbation described by the Hamiltonian

$$H_I = e \mathbf{r} \cdot \mathbf{E}(\mathbf{r}, t) \quad (2.8)$$

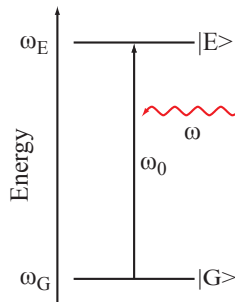


FIGURE 2.1. Energy schematic of an atom with two energy levels separated by an energy of ω_0 which is being radiated with light with energy ω .

where e is the electron charge. This Hamiltonian corresponds to the energy of an electric dipole $-e\mathbf{r}$ in an electric field where \mathbf{r} is the position of the electron with respect to the atom's center of mass. Effectively this interaction Hamiltonian couples the two atomic states with energies ω_G and ω_E if the frequency of radiation ω lies close to the atomic resonance. The next step is to determine the coefficients c_i . To do so we substitute equation 2.5 into the time-dependent Schrödinger equation 2.1

$$\begin{aligned} i\hbar \frac{\partial}{\partial t} (c_G |G\rangle e^{-i\omega_G t} + c_E |E\rangle e^{-i\omega_E t}) &= (H_0 + H_I) (c_G |G\rangle e^{-i\omega_G t} + c_E |E\rangle e^{-i\omega_E t}) \\ \Rightarrow i\hbar (\dot{c}_G |G\rangle e^{-i\omega_G t} + \dot{c}_E |E\rangle e^{-i\omega_E t} - i\omega_G c_G |G\rangle e^{-i\omega_G t} - i\omega_E c_E |E\rangle e^{-i\omega_E t}) &= (H_0 + H_I) (c_G |G\rangle e^{-i\omega_G t} + c_E |E\rangle e^{-i\omega_E t}) \end{aligned} \quad (2.9)$$

Now multiplying the left side with $\langle G|$ and using the orthogonality properties between the wavefunctions, we get

$$\begin{aligned} i\hbar \dot{c}_G e^{-i\omega_G t} + c_G E_G e^{-i\omega_G t} &= c_G E_G e^{-i\omega_G t} + c_E e^{-i\omega_E t} \langle G| H_I |E\rangle \\ \Rightarrow i\dot{c}_G &= c_E e^{-i(\omega_E - \omega_G)t} \cos(\omega t) \frac{\langle G| e\mathbf{r} \cdot \mathbf{E}_0 |E\rangle}{\hbar} \end{aligned} \quad (2.10)$$

Doing the same manipulations but now multiplying from the left with $\langle E|$ gives us the set of coupled differential equations

$$i\dot{c}_G = c_E e^{-i\omega_0 t} \cos(\omega t) \Omega \quad (2.11a)$$

$$i\dot{c}_E = c_G e^{i\omega_0 t} \cos(\omega t) \Omega^* \quad (2.11b)$$

where $\omega_0 = \omega_E - \omega_G$ and Ω is called the Rabi frequency which is defined as

$$\Omega = \frac{\langle G| e\mathbf{r} \cdot \mathbf{E}_0 |E\rangle}{\hbar} = \frac{e}{\hbar} \int \psi_G^* \mathbf{r} \cdot \mathbf{E}_0 \psi_E d^3 r \quad (2.12)$$

If the wavelength of the light is much larger than the size of the atom, $\lambda \gg a_0$, we can assume that variations of the phase $\mathbf{k} \cdot \mathbf{r}$ are small over the atom and the amplitude of the electric field is uniform over the atom so that it can be taken outside the integral. This is called the dipole approximation [10]¹. Thus, for linearly polarized light along the x -axis the Rabi frequency becomes

$$\Omega = \frac{e X_{GE} |\mathbf{E}_0|}{\hbar} \quad (2.13)$$

where X_{GE} is the matrix element for transitions between the ground and excited state. This matrix elements have been measured and can be looked up for most alkali metals. Now to solve the coupled differential equations 2.11a and 2.11b further approximations need to be made[10].

2.1.2.1. The rotating wave approximation. A first approximation we can make for solving the differential equations 2.11a and 2.11b is to assume that all the population starts out in the ground state, $c_G(0) = 1$ and $c_E(0) = 0$. If we then just do the integration we get

$$c_G(t) \simeq 1 \quad (2.14a)$$

$$c_E(t) \simeq \frac{\Omega^*}{2} \left(\frac{1 - e^{i(\omega_0 + \omega)t}}{(\omega_0 + \omega)} + \frac{1 - e^{i(\omega_0 - \omega)t}}{(\omega_0 - \omega)} \right) \quad (2.14b)$$

As a first order approximation this is a reasonable result while $c_E(t)$ remains small (equality 2.6 has to be satisfied). For most cases of interest the radiation has a frequency close to the atomic resonance at ω_0 which means that the magnitude of the detuning is small, $|\omega_0 - \omega| \ll \omega_0$ and of course $\omega_0 + \omega \approx 2\omega_0$. Therefore we can neglect the first term in equation (2.14b) because it is small compared to the term with $\omega_0 - \omega$ in the denominator. This is called the *rotating wave approximation*. The probability of

¹This is actually a bit redundant since the interaction Hamiltonian (equation (2.8)) is already only valid in this approximation.

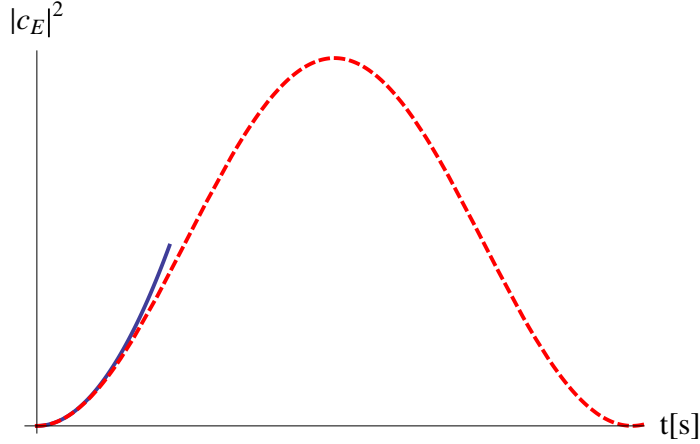


FIGURE 2.2. The blue curve is shows the evolution of the population in the excited state according to equation (2.17) and is only valid for short times. The red dashed curve is shows the evolution of the population in the excited state for longer times and is derived in section (2.1.2.2).

finding an atom in the upper state at time t is given by the modulus squared of the *co-rotating* term

$$|c_E(t)|^2 = \left| \frac{\Omega^*}{2} \frac{1 - e^{i(\omega_0 - \omega)t}}{(\omega_0 - \omega)} \right|^2 \quad (2.15)$$

Which we can rewrite as

$$|c_E(t)|^2 = |\Omega|^2 \frac{\sin^2((\omega_0 - \omega)t/2)}{(\omega_0 - \omega)^2} \quad (2.16)$$

$$|c_E(t)|^2 \underset{|\omega_0 - \omega| \rightarrow 0}{\approx} |\Omega|^2 \frac{t^2}{4} \quad (2.17)$$

So for small t we see that the population in the excited state increases quadratically with time (figure (2.2)).

2.1.2.2. Rabi oscillations. In the derivation of equation 2.14b we assumed that the atom was perturbed only slightly and almost all the population stayed in the ground state. We shall now try to find a solution to the coupled differential equations 2.11a and 2.11b without assuming weak field perturbation. The first step is to write the cosine term in the equations (2.11) as complex exponentials which gives

$$i\dot{c}_G = \frac{\Omega c_E}{2} \left(e^{i(\omega - \omega_0)t} + e^{-i(\omega + \omega_0)t} \right) \quad (2.18a)$$

$$i\dot{c}_E = \frac{\Omega^* c_G}{2} \left(e^{i(\omega + \omega_0)t} + e^{-i(\omega - \omega_0)t} \right) \quad (2.18b)$$

Now we again invoke the rotating wave approximation by assuming that the term containing $(\omega + \omega_0)t$ oscillates very fast and thus averages out over the time of interaction. This leads to the equations

$$i\dot{c}_G = \frac{\Omega}{2} c_E e^{i(\omega - \omega_0)t} \quad (2.19a)$$

$$i\dot{c}_E = \frac{\Omega^*}{2} c_G e^{-i(\omega - \omega_0)t} \quad (2.19b)$$

It is a simple algebraic exercise to combine these which results in the following second order differential equations

$$\ddot{c}_G - i(\omega - \omega_0)\dot{c}_G + \left|\frac{\Omega}{2}\right|^2 c_G = 0 \quad (2.20a)$$

$$\ddot{c}_E + i(\omega - \omega_0)\dot{c}_E + \left|\frac{\Omega}{2}\right|^2 c_E = 0 \quad (2.20b)$$

By solving differential equation 2.20b for the initial conditions $c_G(0) = 1$ and $c_E(0) = 0$ we can find the probability of finding an atom in the excited state as

$$\begin{aligned} |c_E(t)|^2 &= \frac{\Omega^2}{\Omega^2 + (\omega - \omega_0)^2} \sin^2\left(\sqrt{\Omega^2 + (\omega - \omega_0)^2} \frac{t}{2}\right) \\ &= \frac{\Omega^2}{\mathcal{W}^2} \sin^2\left(\mathcal{W} \frac{t}{2}\right) \end{aligned} \quad (2.21)$$

where $\mathcal{W} \equiv \sqrt{\Omega^2 + \delta^2}$ and $\delta = \omega - \omega_0$ is the detuning of the laser light from atomic resonance. Again looking at the case of perturbing the atom with resonant radiation the previous equation reduces to

$$|c_E(t)|^2 = \sin^2\left(\frac{\Omega}{2}t\right) \quad (2.22)$$

The conclusion that we can draw from this relation is that the population oscillates between the ground and excited state [10]. The difference with the result of illuminating an atom with broadband radiation or high powers comes from the fact that this is a perturbative model and does not take into account spontaneous emission. Also with monochromatic light the population saturates (appendix B). Moreover when $\Omega t = \pi = \tau_\pi$ all the atoms have been transferred to the excited state and when $\Omega t = 2\pi$ all the population has returned to the ground state. A pulse in which all the population is transferred is called a π -pulse. These *Rabi oscillations* have been observed in different spectroscopy experiments.

2.2. Density matrix formalism for the two level system

A different way of describing the two level system discussed in the previous section is to make use of the density matrix. The density matrix provides a powerful more tool for doing calculations than the wavefunction approach [11]. In this section we introduce the basic concepts of the density matrix and apply it to the two level system. In this formalism we are able to incorporate the effect of spontaneous emission in a phenomenological way. This will prove to be useful in the next section when we introduce the scattering force. The rate equations describing the evolution of the populations including the spontaneous emission is described in the last part of this section.

2.2.1. Basic concepts. All information about a quantum mechanical system in a pure state is stored in Ψ , however in an experiment Ψ cannot be measured directly. One can only determine the expectation value of a set of quantum mechanical operators \mathcal{A} given by

$$\langle \mathcal{A} \rangle = \langle \Psi | \mathcal{A} | \Psi \rangle \quad (2.23)$$

when Ψ is normalized as $\langle \Psi | \Psi \rangle = 1$.

An alternative way to describe the system is to use the density operator ρ which is given by

$$\rho = |\Psi\rangle\langle\Psi| \quad (2.24)$$

The density operator ρ can be written in terms of an $n \times n$ density matrix, where n is the number of wave functions that completely span the Hilbert space. In most cases the wavefunction Ψ can be

expanded in a basis $\{\phi_n\}$ similar to what we have done in equation (2.2)

$$\Psi = \sum_{i=1}^n c_i \phi_i \quad (2.25)$$

From this definition it follows that the elements of the density matrix become

$$\rho_{ij} = \langle \phi_i | \rho | \phi_j \rangle = \left\langle \phi_i \left| \sum_{i=1}^n c_i \phi_i \right. \right\rangle \left\langle \sum_{k=1}^n c_k \phi_k \left| \phi_j \right. \right\rangle = c_i c_j^* \quad (2.26)$$

In our case of the two level system the elements of the density matrix are

$$\rho_{EE} = \langle E | \rho | E \rangle = \langle E | \Psi \rangle \langle \Psi | E \rangle = |c_E|^2 \quad (2.27a)$$

$$\rho_{GG} = \langle G | \rho | G \rangle = \langle G | \Psi \rangle \langle \Psi | G \rangle = |c_G|^2 \quad (2.27b)$$

$$\rho_{EG} = \langle E | \rho | G \rangle = \langle E | \Psi \rangle \langle \Psi | G \rangle = c_E c_G^* = \rho_{GE}^* \quad (2.27c)$$

And the density matrix is given by

$$\rho = \begin{pmatrix} \rho_{EE} & \rho_{EG} \\ \rho_{GE} & \rho_{GG} \end{pmatrix} \quad (2.28)$$

In this case the normalization condition becomes $\text{Tr}(\rho) = |c_E|^2 + |c_G|^2 = \langle \Psi | \Psi \rangle = 1$. The diagonal elements of the density matrix represent the populations in the excited and the ground state and the off-diagonal elements are called the coherence's since they depend on the phase difference between c_E and c_G [11]. Furthermore the expectation value of an operator \mathcal{A} now becomes

$$\langle \mathcal{A} \rangle = \left\langle \sum_{i=1}^n c_i \phi_i | \mathcal{A} | \sum_{i=1}^n c_i \phi_i \right\rangle = \sum_{i,j} \rho_{ij} \mathcal{A}_{ij} = \sum_j (\rho \mathcal{A})_{jj} = \text{Tr}(\rho \mathcal{A}) \quad (2.29)$$

One can see that if the wavefunction is multiplied by an arbitrary phase factor $e^{i\alpha}$ that there is no change of the expectation value as well as for ρ as is required for an observable [11].

From equation (2.24) we can see that ρ is hermitian so instead of having $2n^2$ real parameters there are only n^2 independent elements. Furthermore the expansion coefficients c_i that determine the wavefunction Ψ contain only $2n - 1$ parameters apart from the overall phase. This reduction in parameters arises because the system is in a pure state² which means that there is a fixed relation between the diagonal and off-diagonal elements³. Alternative to a pure state is a statistical mixture of several states $\{\Psi_n\}$ that can no longer be specified by just a single wavefunction. The density matrix in this case becomes

$$\rho = \sum_i p_i |\Psi_i\rangle \langle \Psi_i| \quad (2.30)$$

²In quantum mechanics there is preference for systems of which there is maximum knowledge. For example for a free particle without spin at a certain time this is the wavefunction $\Psi(x, y, z)$. For an electron in a central potential field this is the state with quantum numbers (n, l, j, m) . States about which there is "maximum knowledge" are also called pure states [?]. More formally let there exist a certain quantum mechanical system for which there is a complete set of commuting operators (whether this is the case depends on the system under study). Then with one single measurement with each operator completely determines the system. Because all the operator commute any subsequent measurement of any of the operators gives the same outcome as the first measurement. If a system is prepared in this way it is called a pure state, or a state of "maximum knowledge" [11].

³The system under discussion here is the two-level atom model that we discussed in the previous section. The two level system system can be described by a the single wavefunction Ψ . Since the overall phase of the wavefunction has no physical meaning there are only three parameter required to describe the wavefunction, c_E , c_G and a relative phase between them [?, 11]. The Hamiltonian in equation (2.1) determines the evolution of the system such that we can predict the outcome. Or at any time one can measure a the expectation value quantum mechanical operator such that it can be predicted. One can than also say that the system is in a pure state.

This relation has the intuitive meaning that the system is in state i with probability p_i . Here there is no longer a relation between the diagonal and off-diagonal terms and complete information on the system now requires n^2 independent elements of the density matrix [11].

The next step is to look for the time dependence of ρ in order to determine the rate equations for the populations of the energy levels. By using the time dependent Schrödinger equation (2.1) one can obtain

$$\begin{aligned}\frac{d}{dt}\rho(t) &= \left(\frac{d}{dt}|\Psi(t)\rangle\right)\langle\Psi(t)| + |\Psi(t)\rangle\left(\frac{d}{dt}\langle\Psi(t)|\right) \\ &= \frac{1}{i\hbar}H(t)|\Psi(t)\rangle\langle\Psi(t)| - \frac{1}{i\hbar}|\Psi(t)\rangle\langle\Psi(t)|H(t) \\ i\hbar\frac{d}{dt}\rho(t) &= [H(t), \rho(t)]\end{aligned}\quad (2.31)$$

This relation is called the **Liouville** equation [?]. This equation points out the special role of ρ in quantum mechanics and is more general than the Schrödinger equation because it can describe pure states as well as statistical mixtures.

To summarize, there are several advantages of using the density matrix formalism versus the wavefunction formalism. The first one is that it eliminates the overall phase, secondly it establishes a more direct connection with observable quantities and it provides a powerful method for doing calculations. In addition it can handle pure states as well as mixed states. This is important to incorporate spontaneous emission in the equation where a pure state is converted to a mixed state [11].

2.2.2. Two level system and the density matrix approach. The evolution equation for the terms ρ_{ij} of the density matrix can now be found for the case of the atom interacting with laser light. For instance by applying equation (2.19a) and (2.19b) in terms of δ we find that

$$\begin{aligned}\frac{\partial\rho_{GG}}{\partial t} &= \frac{\partial c_G}{\partial t}c_G^* + c_G\frac{\partial c_G^*}{\partial t} \\ &= \frac{\Omega}{2i}e^{i\delta t}c_Ec_G^* - \frac{\Omega^*}{2i}e^{-i\delta t}c_Gc_E^* \\ &= \frac{\Omega}{2i}e^{i\delta t}\rho_{EG} - \frac{\Omega^*}{2i}e^{-i\delta t}\rho_{GE}\end{aligned}\quad (2.32)$$

Now lets apply the following transformations

$$\tilde{\rho}_{GE} = \rho_{GE}e^{-i\delta t} \quad (2.33a)$$

$$\tilde{\rho}_{EG} = \rho_{EG}e^{i\delta t} \quad (2.33b)$$

$$\tilde{\rho}_{GG} = \rho_{GG} \quad (2.33c)$$

$$\tilde{\rho}_{EE} = \rho_{EE} \quad (2.33d)$$

We find that

$$\dot{\tilde{\rho}}_{GG} = \frac{\Omega}{2i}(\tilde{\rho}_{EG} - \tilde{\rho}_{GE}) \quad (2.34)$$

In exactly the same way the off diagonal elements of the density matrix can be found, for example

$$\begin{aligned}\dot{\tilde{\rho}}_{GE} &= \frac{d}{dt}\rho_{GE}e^{-i\delta t} \\ &= \frac{d}{dt}c_Gc_E^*e^{-i\delta t} \\ &= \frac{\Omega}{2i}c_Ec_E^* - \frac{\Omega}{2i}c_Gc_G^* - i\delta c_Gc_E^*e^{-i\delta t} \\ &= \frac{\Omega}{2i}(\tilde{\rho}_{EE} - \tilde{\rho}_{GG}) - i\delta\tilde{\rho}_{GE}\end{aligned}\quad (2.35)$$

This leads to the in total four equations

$$\dot{\tilde{\rho}}_{GG} = \frac{\Omega}{2i} (\tilde{\rho}_{EG} - \tilde{\rho}_{GE}) \quad (2.36a)$$

$$\dot{\tilde{\rho}}_{EE} = -\frac{\Omega}{2i} (\tilde{\rho}_{EG} - \tilde{\rho}_{GE}) \quad (2.36b)$$

$$\dot{\tilde{\rho}}_{EG} = -\frac{\Omega}{2i} (\tilde{\rho}_{EE} - \tilde{\rho}_{GG}) + i\delta\tilde{\rho}_{EG} \quad (2.36c)$$

$$\dot{\tilde{\rho}}_{GE} = \frac{\Omega}{2i} (\tilde{\rho}_{EE} - \tilde{\rho}_{GG}) - i\delta\tilde{\rho}_{GE} \quad (2.36d)$$

These equations are also called the optical Bloch equations. They can be extended to include spontaneous emissions as we shall see in the next section. These equations give the time evolutions of a two level system which is driven by resonant light analogue to what we saw in section 2.1. Using the *Bloch vector* these equations give an intuitive picture of the time development of the two level system

2.2.2.1. The Bloch vector. In equations (2.36) there are only three free parameters. These three parameters are the three components of the Bloch vector $\mathbf{R} = (U, V, W)$

$$U = \tilde{\rho}_{EG} + \tilde{\rho}_{GE} \quad (2.37a)$$

$$V = i(\tilde{\rho}_{EG} - \tilde{\rho}_{GE}) \quad (2.37b)$$

$$W = \tilde{\rho}_{GG} - \tilde{\rho}_{EE} \quad (2.37c)$$

Using these definitions we can write the optical Bloch equations as

$$\dot{U} = \frac{\dot{\tilde{\rho}}_{EG} + \dot{\tilde{\rho}}_{GE}}{2} = \delta V \quad (2.38a)$$

$$\dot{V} = -\delta U - \Omega W \quad (2.38b)$$

$$\dot{W} = \Omega V \quad (2.38c)$$

These equations can be written in vector notation as

$$\dot{\mathbf{R}} = \mathbf{R} \times (\Omega \hat{\mathbf{e}}_1 + \delta \hat{\mathbf{e}}_3) = \mathbf{R} \times \mathbf{W} \quad (2.39)$$

by defining the vector \mathbf{W} as

$$\mathbf{W} = \Omega \hat{\mathbf{e}}_1 + 0 \hat{\mathbf{e}}_2 + \delta \hat{\mathbf{e}}_3 \quad (2.40)$$

which has magnitude $W = \sqrt{\Omega^2 + \delta^2}$ and which we recognize from equation (2.21). Because $\dot{\mathbf{R}}$ is orthogonal to both \mathbf{R} and \mathbf{W} the magnitude $|\mathbf{R}|^2$ is constant and unity⁴. The Bloch vector corresponds to the position vector of point on the surface of a sphere with a radius of unity which is called the Bloch sphere. In this picture the vector \mathbf{R} precesses around the vector \mathbf{W} where the magnitude of \mathbf{R} is preserved. This picture was first proposed in a paper by Feynman, Vernon and Hellwarth [12]. The vector \mathbf{W} acts as a three component vector that determines the rate and axis of precession. In this picture all possible quantum state of the two level system are projected on the surface of the Bloch sphere. It is the usual convention to define the \mathbf{W} -axis as the z -axis. Then at the south pole of the sphere the atom is in the ground state and in the north pole the atom is in the excited state. All points besides these represent superpositions of the ground and excited state [10].

All situations can now be intuitively described by looking at the Bloch sphere. In the case of large detunings, i.e. $\delta \gg 1$ the precession is near the poles and the system remains either in the ground or in the excited state. Resonant excitation, i.e. $\delta = 0$ gives $\mathbf{W} = \Omega \hat{\mathbf{e}}_1$ in equation (2.40) and \mathbf{R} describes a cone around $\hat{\mathbf{e}}_1$. In the case that all the population starts out in the ground state the Bloch vector rotates in the plane perpendicular to $\hat{\mathbf{e}}_1$ mapping out a circle on the Bloch sphere. This motion corresponds to the Rabi oscillations from equation (2.22).

⁴This can also be shown by writing U , V and W in terms of the coefficients c_G and c_E .

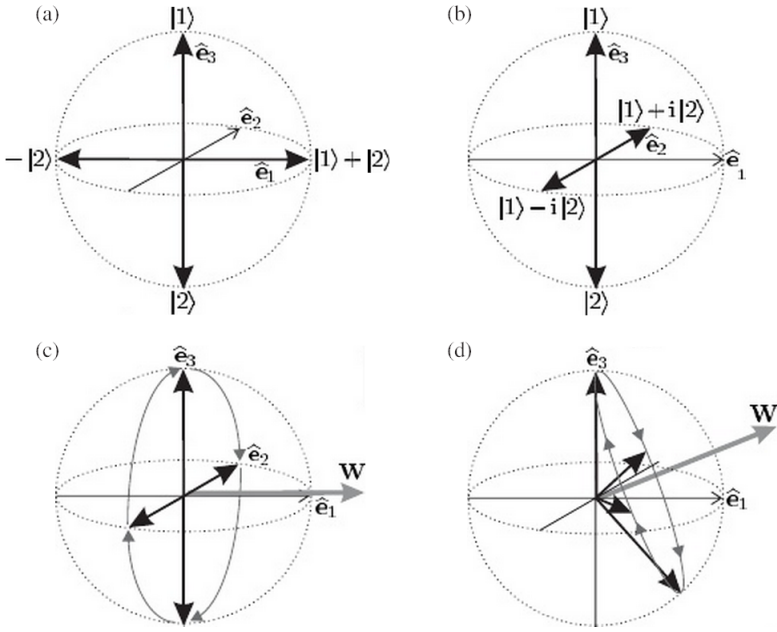


FIGURE 2.3. The Bloch sphere. The position of vectors of point on the surface represent states of the two-level system. Two examples of possible states are given in (a) and (b). The poles represent special states where the atom is either in the ground state or in the excited state. All possible states can be represented as a point on the Bloch sphere. Figure from [10].

2.2.3. Spontaneous emission. Spontaneous emission results in a transition of the system from an initial to a final state and can convert a pure state to a statistical mixture. The fact that the system is a statistical mixture is in this case not a consequence of incomplete preparation of the system but it is due to partial detection of the final state. Consider a two level atom in the excited state and no photons in the radiation field. This system is in a pure state $|E, 0\rangle$ where the first parameter describes the state of the system and the second the fact that there are no photons in the radiation field. This system now makes a transition from the excited state to the ground state by emitting a photon on the radiation field. This state is denoted by $|G, 1_S\rangle$ where $S = (\mathbf{k}, \varepsilon)$ is the mode of the spontaneous emission which we can now describe by the wavefunction

$$\Psi(t) = c_{E,0} e^{-i\omega_E t} |E, 0\rangle + \sum_S c_{G,1_S} e^{-i(\omega_G + \omega)t} |G, 1_S\rangle \quad (2.41)$$

where the sum is over all possible modes S . This means that the photon can be emitted in all directions with a certain polarization. If one only observes the state of the atom and not the photon, then the atom is found in either the ground or the excited state however it no longer is a pure state.

We can add the dissipative effects phenomenologically in the Schrodinger picture by incorporating an extra term in equation (2.19b) to describe the decay of the excited state population

$$i\dot{c}_E = \frac{\Omega^*}{2} c_G e^{-i\delta t} - \frac{\Gamma_E}{2} c_E \quad (2.42)$$

Without coupling to the laser field ($\Omega = 0$) the relaxation terms gives an exponential decay of the excited level population

$$|c_E(t)|^2 = |c_E(0)| e^{-\Gamma_E t} \quad (2.43)$$

In the optical Bloch equations this leads to the extra term of

$$\dot{\rho}_{ij} = (\dot{\rho}_{ij})_{\text{no dissipation}} - \frac{\Gamma_i + \Gamma_j}{2} \rho_{ij} \quad (2.44)$$

This relations gives the exponential decay of the population of a state. Since Γ_i describes the spontaneous decay we see that $\Gamma_i \rho_{ii}$ is the rate of spontaneous emission. The excited state population decays as

$$\dot{\rho}_{EE} = -\Gamma_E \rho_{EE} \quad (2.45)$$

while the ground state population increases at the same rate

$$\dot{\rho}_{GG} = \Gamma_E \rho_{GG} \quad (2.46)$$

One can also show that the off diagonal terms of the matrix decay as

$$\dot{\rho}_{EG} = -\frac{\Gamma_E}{2} \rho_{EG} \quad (2.47)$$

We can thus add these loss terms in the equations of motion, equation (2.31), as

$$i\hbar \frac{d}{dt} \rho(t) = [H(t), \rho(t)] - \frac{1}{2} \{\Gamma, \rho\}$$

which leads optical Bloch equations including spontaneous emission ($\Gamma_{EE} = \Gamma$)

$$\dot{\tilde{\rho}}_{GG} = \frac{\Omega}{2i} (\tilde{\rho}_{EG} - \tilde{\rho}_{GE}) + \Gamma \tilde{\rho}_{EE} \quad (2.48a)$$

$$\dot{\tilde{\rho}}_{EE} = -\frac{\Omega}{2i} (\tilde{\rho}_{EG} - \tilde{\rho}_{GE}) - \Gamma \tilde{\rho}_{EE} \quad (2.48b)$$

$$\dot{\tilde{\rho}}_{EG} = -\frac{\Omega}{2i} (\tilde{\rho}_{EE} - \tilde{\rho}_{GG}) + \left(\frac{\Gamma}{2} + i\delta \right) \tilde{\rho}_{EG} \quad (2.48c)$$

$$\dot{\tilde{\rho}}_{GE} = \frac{\Omega}{2i} (\tilde{\rho}_{EE} - \tilde{\rho}_{GG}) - \left(\frac{\Gamma}{2} - i\delta \right) \tilde{\rho}_{GE} \quad (2.48d)$$

One thing to note in these equations is that $\dot{\tilde{\rho}}_{GG} = -\dot{\tilde{\rho}}_{EE}$ which is according to the requirement of a closed two level system where the population is normalized according to $\rho_{GG} + \rho_{EE} = 1$. Furthermore it is assumed that the decay of the coherence's and the decay of the excited stated are described by the single parameter Γ . For the discussion throughout this thesis this is always the case, however when collisions between atoms start to play a role the decay of the coherence's and the populations are described by different decay parameters [?].

2.3. Laser cooling and trapping

Trapping and cooling of atoms using light rely on the light to exert a controllable force on the atoms. The beginning of this section introduces the force of a single frequency light beam on a two level atom. The description is in one dimension and shows how absorption of photons from the atom alters the velocity of the atoms. The mechanism is based on the interaction between a two level atom and light described in the previous sections. After the introduction of this *light force* a specific application is introduced: *the optical molasses technique*. This technique is based on the principles of the force light exerts on atoms and can be used to cool down atoms. The final piece of this section describes a trapping mechanism for atoms using light and magnetic field gradients called the *magneto optical trap*.

2.3.1. Scattering force. The notion that light (radiation) has momentum dates back to the Maxwell in the nineteenth century. The idea is simple and follows from conservation of momentum. When an object adsorbs radiation its momentum changes something first observed by Compton in 1925 [10]. Consider an atom of mass M traveling at velocity v that absorbs a photon that travels with

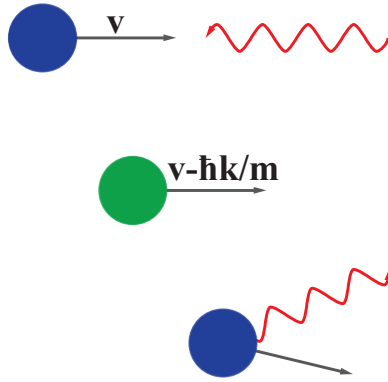


FIGURE 2.4. An atom moving with velocity v to the right that absorbs a photon moving to the left with momentum $p = \hbar k$ changes its velocity by a recoil velocity of $v_R = \hbar k/M$. This absorption is followed by a subsequent spontaneous emission which is in a random direction.

velocity opposite to the velocity of the atom as depicted in figure 2.4. Conservation of momentum dictates that

$$\hbar \mathbf{k}_i + M \mathbf{v}_i = M (\mathbf{v}_i - \hbar \mathbf{k}_i) = M \mathbf{v}_f \quad (2.49)$$

with photon impulse

$$p = \hbar |\mathbf{k}| = \frac{\hbar \omega}{c} \quad (2.50)$$

The change in the atomic velocity when absorbing or emitting a resonant photon is called the *recoil velocity*. From equation (2.49) we determine this velocity to be

$$|v_R| = \frac{\hbar |\mathbf{k}|}{M} \quad (2.51)$$

Now each absorbed photon gives the atom a kick in the direction opposite to its motion whereas spontaneously emitted photons go in all directions. This means that the scattering of many photons gives you a resulting force that slows down the atoms [10]. The magnitude of the *scattering force* is equal to the rate at which photons are absorbed by the atoms times their momentum

$$F_{\text{scatt}} = \hbar k \Gamma_{\text{scatt}} \quad (2.52)$$

where $\Gamma_{\text{scatt}} = \Gamma \rho_{EE}$ (see equation (2.45)⁵) is the scattering rate and ρ_{EE} is the population in the excited state [11]. The fraction of the population in the excited state is given by

$$\rho_{GG} + \rho_{EE} = 1 \quad (2.53)$$

$$W = \rho_{GG} - \rho_{EE} \quad (2.54)$$

$$\Rightarrow \rho_{EE} = \frac{1 - W}{2} \quad (2.55)$$

where W is given by (B.2) (appendix B). Substitute this equation to obtain

$$F_{\text{scatt}} = \frac{\hbar k \Gamma}{2} \frac{\Omega^2/2}{\delta^2 + \Omega^2/2 + \Gamma^2/4} \quad (2.56)$$

or in terms of the saturation intensity (see appendix B)

$$F_{\text{scatt}} = \frac{\hbar k \Gamma}{2} \frac{I/I_S}{1 + I/I_S + (2\delta/\Gamma)^2} \quad (2.57)$$

⁵Of course the rate at which atoms decay spontaneously is equal to rate at which photons are absorbed in steady state

When $I \rightarrow \infty$ the force has a limiting value of $F_{\max} = \hbar k \Gamma / 2$. This shows, looking at equation (2.52), that the scattering rate Γ_{scatt} tends to $\Gamma/2$ which makes sense since we showed (Appendix B) that at high intensities the populations in the upper level and lower level both approach $1/2$.

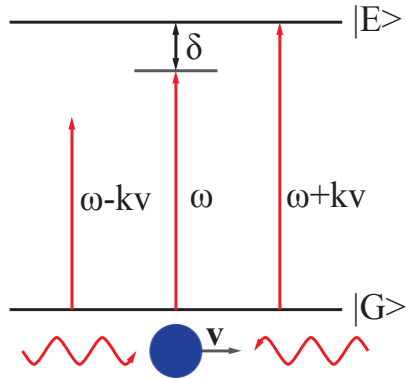


FIGURE 2.5. An atom radiated by two opposing laser beams that are red-detuned "sees" a frequency shift of the laser toward atomic resonance of the laser beam counter opposite to its speed. This Doppler induced frequency shift causes atoms to scatter more light from the beam it is moving towards resulting in a velocity dependent force.

2.3.2. Optical molasses. The light force described above can be used to cool down atoms. The possibility of cooling down atom using the scattering force has its origin in the strong frequency dependence of atomic absorption near resonance. Due to the Doppler effect the laser frequency "seen" by atoms changes as a function of their speed. Of course a velocity dependent dissipative force is needed in order to cool down atoms. The first application of this light force is to aim a laser beam, with a frequency below atomic resonance, opposite to an atomic beam. In the reference frame of the atoms moving towards the light the frequency has increased due to the Doppler effect. Because the frequency seen by the atoms increases it is closer to atomic resonances and the rate of absorption increases see figure 2.5. The result is a force that slows the atom down depending on the velocity of the atom.

So let's now extend the discussion to include the radiative force from more than one beam. For example, if we direct two laser beams with equal intensity, polarization and low enough intensity opposite to each other the net force is given by adding equation (2.57) for both of the beams. Obviously for an atom at rest nothing happens but an atom moving in the direction of one of the beams feels a force proportional to its velocity. If the laser is tuned below the atomic resonance (red detuning) atoms interact more strongly with the light propagating opposite to their speed and they will slow down. By using two opposing beams in all three directions atoms are slowed down in all directions and many atoms can be cooled inside a small volume. The force, in one dimension, can be calculated under the assumption that the intensity is low enough that stimulated emission can be neglected. In

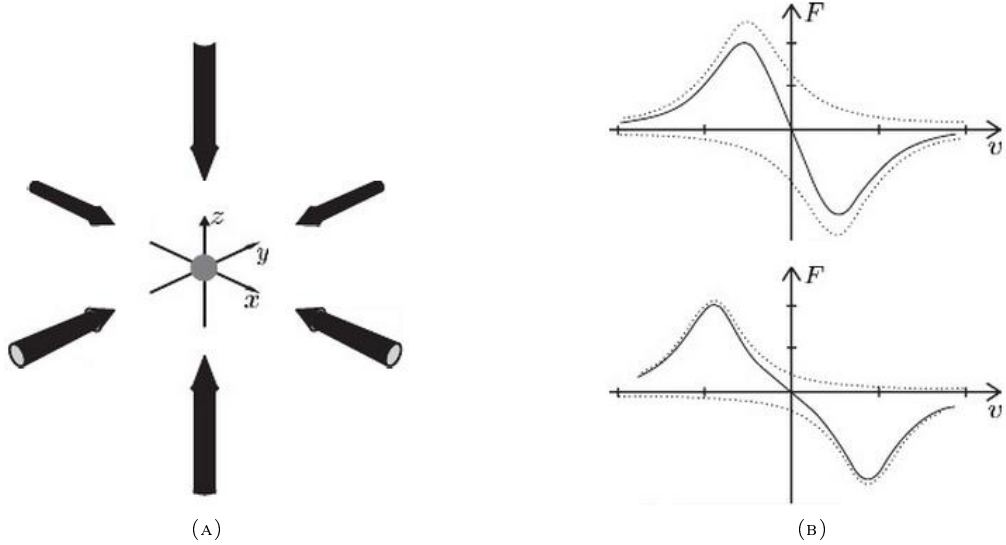


FIGURE 2.6. The technique that uses six orthogonal counter propagating laser beams is called the optical molasses technique, depicted in (A). The laser beams are tuned slightly below atomic resonance. In (B) the force (solid line) in the optical molasses is shown as a function of velocity ($\delta = -\Gamma/2$ for the upper plot and $\delta = -\Gamma$ for the lower plot). The dotted lines represent the force from each of the two beams separately. The damping is proportional to the slope at $v = 0$. Since the force is negative for $v > 0$ and positive for $v < 0$ the atoms are decelerated. Figures were taken from [10].

this case we can just simply add the forces from the two light beams

$$\begin{aligned}
 F_{\text{mol}} &= F_{\text{scatt}}(\delta - kv) + F_{\text{scatt}}(\delta + kv) \\
 &= \frac{\hbar k \Gamma I / I_S}{2} \left(\frac{1}{1 + I/I_S + 4(\delta - \mathbf{k} \cdot \mathbf{v}/\Gamma)^2} + \frac{1}{1 + I/I_S + 4(\delta + \mathbf{k} \cdot \mathbf{v}/\Gamma)^2} \right) \\
 &\approx \frac{8\hbar\delta I / I_S k^2 \mathbf{v}}{\Gamma \left(1 + I/I_S + (2\delta/\Gamma)^2 \right)^2} \\
 &\equiv -\alpha \mathbf{v}
 \end{aligned} \tag{2.58}$$

Where in the third line we neglected terms of order $(kv/\Gamma)^4$ since for low velocities we have $kv \ll \Gamma$. Moreover, from the last line we see that the light exerts a frictional force for low enough velocities. This is basically the same equation for objects moving in a viscous liquid if α is positive, therefore it has been given the name *optical molasses*. For this condition the force is plotted in figure 2.6b and has a negative gradient at $v = 0$. Of course to cool the atoms down in all directions six beams have to be used in total. A typical setup for optical molasses is shown in figure 2.6a.

The description of the force on an atom from two opposite laser beams is only valid for intensities that are low such that absorptive effects can be neglected. If the power becomes too large dipole interaction (section 2.4.1) and optical lattice effects (section 2.4.3) start to become important.

It is important to note that this force is not a trapping force; it just slows down atoms dependent on the speed they have. In order to create the trap there also needs to be a position dependent force which can be obtained by introducing a quadrupole magnetic field. This in combination with light is called a magneto optical trap and is described in section 2.3.3.

2.3.2.1. Doppler cooling limit. If the above described mechanism is all there is to this story the atoms would very quickly decelerate down to $v = 0$ and therefore cool down to $T = 0$. This result

clearly goes against any physical intuition since it violates thermodynamics [11]. It turns out that there is some heating in the system caused by the light beams that we must consider. The origin of this heating comes from the discrete size of momentum steps the atoms undergo when they absorb or emit an photon. Since their momentum changes in steps of $\hbar k$ their kinetic energy changes by at least the recoil energy

$$E_R = \frac{1}{2} M v_R^2 = \frac{\hbar^2 k^2}{2M} = \hbar \omega_R \quad (2.59)$$

where v_R is given by equation (2.51). This results in the fact that the average frequency of absorption is $\omega_{abs} = \omega + \omega_R$ and the average frequency of emission is $\omega_{emit} = \omega - \omega_R$. So for each scattering the light field loses an energy of $\hbar(\omega_{abs} - \omega_{emit}) = 2\hbar\omega_R$ for each scattering event. For two beams this happens at a rate $2\Gamma_{scatt}$ and the energy becomes kinetic energy. This causes the sample to heat because the recoils are in random directions [11].

The next step is to use the cooling rate $\mathbf{F}_{mol} \cdot \mathbf{v}$ and the heating rate $4\hbar\omega_R\Gamma_{scatt}$ to determine this cooling limit. The change in kinetic energy is given by [11]

$$\frac{1}{2} M \frac{d \langle v^2 \rangle}{dt} = 4\hbar\omega_R\Gamma_{scatt} - \alpha v^2 \quad (2.60)$$

If the two forces are in balance we find an equation for v^2 by setting the time derivative to zero

$$\langle v^2 \rangle = \frac{4E_R\Gamma_{scatt}}{\alpha} \quad (2.61)$$

where equation (2.59) was substituted to get v in terms of the recoil energy. Of course for a configuration with six beams similar equations apply for the velocity in their respective directions. In this derivation we neglected any saturation effects since of course an atom absorbs photons faster if it is illuminated by three times more laser beams. The temperature of this motion along the axis of the beams is related to the temperature (according to the equipartition theorem)

$$\frac{1}{2} M v^2 = \frac{1}{2} k_B T \Rightarrow k_B T = \frac{4ME_R\Gamma_{scatt}}{\alpha} \quad (2.62)$$

where k_B is the Boltzmann constant. If we now substitute Γ_{scatt} and α given by equation (2.57) and (2.58) respectively we find that

$$k_B T = \frac{\hbar\Gamma}{4} \left(\frac{2\delta}{\Gamma} + \frac{\Gamma}{2\delta} \right) \quad (2.63)$$

This equation is dependent on δ and has a minimum at $\delta = -\Gamma/2$. The temperature for this minimum is called the *Doppler cooling limit* and is given by

$$T_{Doppler} = \frac{\hbar\Gamma}{2k_B} \quad (2.64)$$

It is now time to make an small historical note. It was initially presumed that this was the limiting temperature for laser cooling until experimental measurements using this technique found much lower temperatures, especially when the Earth's magnetic field was canceled out. This effect was first measured by the group of William Phillips and presented in 1988 [13]. This effect was understood later and turned out to be inexplicable by just a two level atom (this an example of where our model breaks down). Real alkali atoms have degenerate energy levels which complicates the scheme but is a rare example where things turn out better than in the simplified model. Another important mechanism for cooling is the fact that for circularly polarized light, which is the case for the MOT (see section 2.5), the polarization is spatially not constant. Therefore it has also been given the name polarization gradient cooling. The lowest possible temperature that can be reached using laser cooling is called the recoil limit. Although we do not derive this limit and the theoretical explanation in this thesis a great paper on the subject was written by Dalibard and Tannoudji for further reference [14]. One important

thing to note is the use of the term optical molasses. This term is used throughout this thesis referring to laser cooling also to temperatures below the Doppler limit.

2.3.3. The magneto-optical trap. As was already mentioned in the previous section the optical molasses technique cools down the atoms but it does not trap any atoms⁶. This configuration can however be turned into a trap by adding magnetic fields. This employment of both optical and magnetic fields is called a *magneto-optical trap* (MOT) and is one of the most widely used traps to capture neutral atoms. The use of such a trap was first presented in 1987 by D. Pritchard [11]. The working of the MOT requires inhomogeneous magnetic fields and radiative selection rules (D) to exploit both optical pumping and the strong radiative force [11]. The radiative interaction between the atoms and the light fields provides the cooling mechanism. A MOT trap is very robust and does not rely on the precise balancing of the beams nor is a very high degree of polarization required. The magnetic field gradients that are needed for the trapping force are fairly modest and can be achieved with "simple" air or water cooled coils. It is also easy to construct because it can be operated with a room temperature vacuum system where the alkali atoms are trapped from the vapor. Also, to produce the correct light fields low-cost diodes can be used which has made the MOT one of the least expensive ways to produce atomic samples at temperatures below 1mK [11].

For a simple $F_G = 0$ to $F_E = 1$ transition the principle of the MOT is illustrated in figure 2.7 . The magnetic field gradient that is needed for the MOT is created by two coils with currents running in opposite directions. This creates a quadrupole magnetic field where in the middle of the coils the magnetic field produced cancel out such that $B = 0$ at the center of the trap. Close to the center of the trap the magnetic field has a uniform gradient that perturbs the atomic energy levels. This Zeeman effect causes the energy levels of the $F_E = 1$ to degenerate into three sub-levels with $M_F = 0, \pm 1$ that vary linearly with the atom's position as shown in 2.7. Each of the three Zeeman components is excited by each of three polarizations whose frequencies tune with field (and therefore position). So at a position $z > 0$ the magnetic field tunes the $M_J = -1$ transition closer to resonance and the $M_F = 1$ further from resonance for two counter propagating laser beams with a detuning of δ from atomic resonance. If the polarization is chosen such that the light beam incident from the right is σ_-

⁶The atoms will accumulate in the region where the three orthogonal pairs of beams intersect because it takes a considerable amount of time for the atoms to diffuse out but the force itself is a slowing force and is not dependent on position [10].

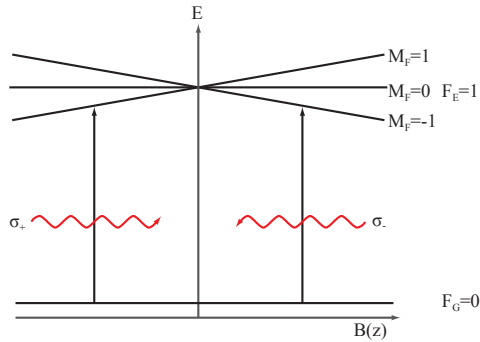


FIGURE 2.7. The basic mechanism for an MOT in this case for an $F_G = 0$ to an $F_E = 1$ transition. Because of the magnetic field gradient the Zeeman splitting of the $F_G = 1$ into three sub levels becomes position dependent. The two counter propagating waves have circularly polarized light and the selection rules (D) lead to an imbalance in the radiative force of the two laser beams that leads to a force pushing the atoms towards the center. Picture taken from [10].

polarized and the light beam from the left is σ_+ polarized more light is scattered from the σ_- beam than from the σ_+ beam. This results in a force that pushes the atoms towards the center of the trap. On the other side of the trap the same thing happens for the $M_F = 1$ state⁷.

In order to describe the MOT mathematically we incorporate the frequency shift due to the Zeeman splitting into equation (2.58) for the optical molasses. We assume small Zeeman shift, $\beta z \ll \Gamma$, small velocities $kv \ll \Gamma$ and still low intensities $I/I_S \ll 1$ which gives the MOT-force as

$$F_{MOT} = F_{\text{scatt}}(\delta + \beta z - kv) + F_{\text{scatt}}(\delta - \beta z + kv) \quad (2.65)$$

where the term $\delta + \beta z$ is the frequency that is resonant with the absorption for the $M_F = 1$ transition at a position z . The Zeeman shift at a position z is given by

$$\beta z = \frac{g\mu_B}{\hbar} \frac{dB}{dz} z \quad (2.66)$$

where $g \equiv (g_{F'}M_{F'} - g_FM_F)$ for a transition between the hyperfine structure levels $|F, M_F\rangle$ and $|F', M_{F'}\rangle$ [11]. Note the similarity between the Doppler shift $\omega_D \equiv -\mathbf{k} \cdot \mathbf{v}$ and the Zeeman shift $\omega_Z \equiv \beta z$ that both have opposite signs for opposite beams. In the limit of small Zeeman shift and small velocities this can be expanded as [10]

$$F_{MOT} \cong -\alpha v - \frac{\alpha\beta}{k} z \quad (2.67)$$

The Zeeman effect causes an imbalance in the radiation force (similar to the way Doppler shift leads to a cooling force) that leads to a restoring force with spring constant $\kappa \equiv \alpha\beta/k$. The force given by equation (2.67) causes the atom to undergo damped harmonic motion with damping rate $\Gamma_{MOT} = \alpha/M$ and oscillation frequency $\omega_{MOT} = \sqrt{\kappa/M}$. Atoms that enter the region where the laser beams intersect are cooled as in the optical molasses technique and the position depend force drives them to the middle of the trap and thus trapping them.

So far the discussion about the MOT has been limited to one dimension however, the MOT can easily be extended to three dimensions using six laser beams, see figure 2.8. Furthermore, even though very few atomic species have transitions as simple as $J = 0 \rightarrow J = 1$ the scheme works for real alkali atoms as well [11]. In section 3.1 a MOT scheme for rubidium atoms is discussed.

In a MOT setup atoms can be cooled below the Doppler limit mentioned in the previous section. However, to reach lower temperatures it is important to cancel out all residual magnetic fields. So although historically optical molasses came before the MOT a typical apparatus uses the MOT to capture atoms from a slowed atomic beam or from a hot background gas (this is the case for our experiment). After this initial capturing and cooling stage the atoms are cooled down further in "just" the optical molasses before any other experiments are carried out [10]. This is also something that we will encounter again in section 3.1.

2.4. The dipole force

So far the discussion of the interaction between light and atoms was focused on the absorption of photons followed by subsequent spontaneous emission. This resulted in a dissipative force on the atoms caused by the momentum transfer of the absorbed and emitted photons. This scattering force can be used to cool down atoms however, in order to trap the atoms an additional magnetic field is needed. This section describes a different way in which light and atoms can interact. There is a conservative component which arises from the interaction of the light field with the induced dipole moment of the

⁷Amongst different literature there exist different definitions of what σ_- and σ_+ polarized light means. In this case σ_+ and σ_- refer to transitions of the atom and labeling the radiation as σ_+ is shorthand for circularly-polarized radiation of the handedness that excites the σ_+ transition. This is a convenient convention for discussing the principles of laser cooling where the transitions that occur depend on the sense of rotation of the electric field around the quantization axis of the atom whereas handedness depends on both the sense of rotation and the direction of the propagation[10].

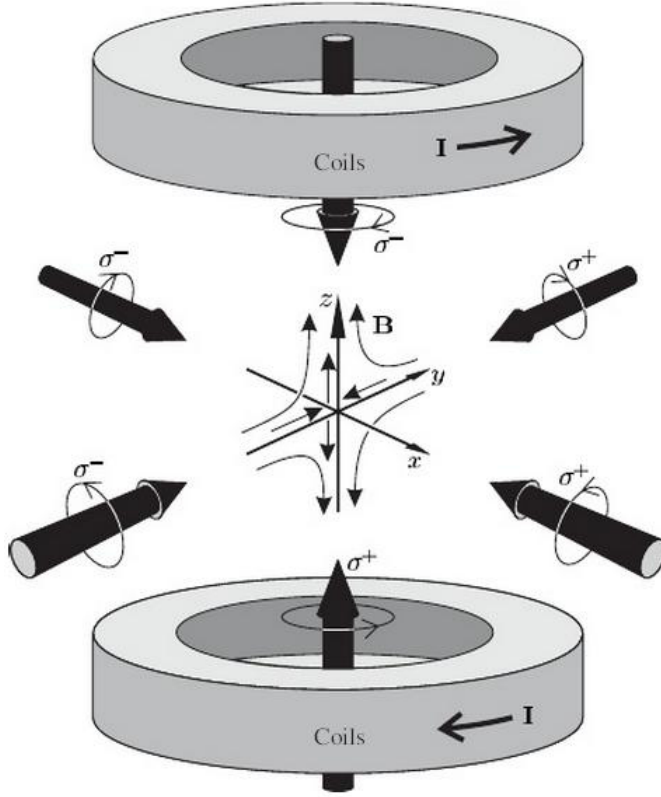


FIGURE 2.8. An magneto-optical trap is build up out of six counter-propagating laser beams that intersect in the middle each with the right polarization. The small arrows indicate the direction of the quadrupole magnetic field produced by two coils with counter-propagating current. This causes the atoms to be pushed towards the center of the trap from all direction. Figure taken from [10]

atom. The interaction with the light field causes a shift in the potential energy which is also referred to as the ac-Stark shift or light shift (C). For large detunings of the light, with respect to the atomic resonance, spontaneous emission processes can be neglected and the energy shift can be used to create a conservative trapping potential for neutral atoms.

In the first part of this section the basic concepts of trapping atoms using *optical dipole potentials* using far-detuned light is introduced. In this regime the scattering of photons can be neglected compared to the dipole force. Secondly the most basic trap for atoms using light is discussed, namely a focused beam trap. Another trap for cold atoms is the lattice potential which is described in the final part of this section and is of particular interest for the second chapter.

2.4.1. Dipole interaction with the light field. In this section we shall not just derive the dipole force on an atom but also the scattering force (the same that was already discussed in previous sections). This more clearly demonstrates the relationship between these two types of forces. The optical dipole force arises from the dispersive interaction of the atomic dipole moment with the intensity gradient of the light field. Because it constitutes a conservative force it can be derived from the potential gradient. The minimum of this potential can be used to trap atoms. The absorptive part of the dipole interaction, the photon scattering, limits the dipole traps [15].

When an atom is placed into laser light, the electric field \mathbf{E} induces an atomic dipole moment \mathbf{p} that oscillates at the driving frequency ω . The electric field and dipole moment are given by

$$\mathbf{E}(\mathbf{r}, t) = \hat{\mathbf{e}}\tilde{E}(\mathbf{r}) e^{-i\omega t} + c.c. \quad (2.68)$$

$$\mathbf{p}(\mathbf{r}, t) = \hat{\mathbf{e}}\tilde{p}(\mathbf{r}) e^{-i\omega t} + c.c. \quad (2.69)$$

where $\tilde{E}(\mathbf{r})$ and $\tilde{p}(\mathbf{r})$ are the complex amplitudes and $\hat{\mathbf{e}}$ is the unit polarization vector. The amplitudes are related to each other by

$$\tilde{p}(\mathbf{r}) = \alpha(\omega)\tilde{E}(\mathbf{r}) \quad (2.70)$$

where α is the complex polarizability which depends on the light frequency ω . The resulting dipole potential is determined by time averaging over $\mathbf{E} \cdot \mathbf{p}$

$$\begin{aligned} U_{\text{dip}} &= -\frac{1}{2}\langle \mathbf{E} \cdot \mathbf{p} \rangle \\ &= -\frac{1}{2}\left\langle \left(\hat{\mathbf{e}}\tilde{E}(\mathbf{r}) e^{-i\omega t} + c.c. \right) \cdot \left(\hat{\mathbf{e}}\tilde{p}(\mathbf{r}) e^{-i\omega t} + c.c. \right) \right\rangle \\ &= -\frac{1}{2}\left\langle \left(\hat{\mathbf{e}}\tilde{E}(\mathbf{r}) e^{-i\omega t} + c.c. \right) \cdot \left(\hat{\mathbf{e}}\alpha(\omega)\tilde{E}(\mathbf{r}) e^{-i\omega t} + c.c. \right) \right\rangle \\ &= -\frac{1}{2}\left| \tilde{E}(\mathbf{r}) \right|^2 (\alpha + \alpha^*) \end{aligned} \quad (2.71)$$

Here the factor $1/2$ does not occur for a permanent dipole [10]. The intensity of the light field is given by

$$I = 2\epsilon_0 c |\mathbf{E}|^2 \quad (2.72)$$

Substituting this equation into equation⁸ 2.71

$$U_{\text{dip}} = -\frac{I}{2\epsilon_0 c} \frac{1}{2} (\alpha + \alpha^*) = -\frac{1}{2\epsilon_0 c} \text{Re}(\alpha) I \quad (2.73)$$

The potential energy is thus proportional to the intensity of the light field and the real part of the polarizability. This describes the in-phase component of the dipole interaction which is cause for the dispersive properties of the interaction [15]. Because it is a conservative force it can be derived from the potential. The dipole force is found by taking the gradient of the last equation where the intensity of the laser field is dependent on \mathbf{r}

$$\mathbf{F}_{\text{dip}}(\mathbf{r}) = -\nabla U_{\text{dip}}(\mathbf{r}) = \frac{1}{2\epsilon_0 c} \text{Re}(\alpha) \nabla I(\mathbf{r}) \quad (2.74)$$

From this one can conclude that the dipole force is proportional to the intensity gradient of the applied light field.

The quality of the trap is limited by the absorptive part of the interaction. Lets consider the light as a stream of photons $\hbar\omega$, then the absorption of power by the oscillator from the driving field can be interpreted in terms of photon scattering in cycles of absorption and spontaneous re-emission [15]. The scattering rate is then given by

$$\Gamma_{\text{sc}}(\mathbf{r}) = \frac{1}{\hbar\omega} P_{\text{abs}} \quad (2.75)$$

where P_{abs} is given by

$$P_{\text{abs}} = \frac{d}{dt} U_{\text{dip}} \quad (2.76)$$

⁸ $\text{Re}(z) = \frac{1}{2}(z + \bar{z})$

Using the relation between the amplitudes of the dipole moment and electric field given in equation (2.70) this becomes

$$\begin{aligned} P_{\text{abs}} &= \langle \hat{\mathbf{p}} \cdot \mathbf{E} \rangle \\ &= \left\langle -i\omega \tilde{p}(\mathbf{r}) \tilde{E}(\mathbf{r})^* + i\omega \tilde{E}(\mathbf{r})^* \tilde{p}(\mathbf{r}) \right\rangle \\ &= 2\omega \left| \tilde{E}(\mathbf{r}) \right|^2 \text{Im}(\alpha) \end{aligned} \quad (2.77)$$

Using equation (2.72) for the laser field intensity the scattering rate becomes

$$\Gamma_{\text{sc}}(\mathbf{r}) = \frac{P_{\text{abs}}}{\hbar\omega} = \frac{1}{\hbar\epsilon_0 c} \text{Im}(\alpha) I(\mathbf{r}) \quad (2.78)$$

The two main quantities of interest for dipole traps, dipole potential and scattering rate, are expressed in terms of the laser field intensity and the atomic polarizability. We see that the dipole potential is proportional to the real part of the polarizability which is responsible for the dispersive properties of the interaction. On the other hand we see that the scattering rate is proportional to the imaginary part of the polarizability which is responsible for the absorptive part of the interaction. The atomic polarizability is given by [15]

$$\alpha(\omega) = 6\pi\epsilon_0 c^3 \frac{\Gamma/\omega_0^2}{\omega_0^2 - \omega^2 - i(\omega^3/\omega_0^2)\Gamma} \quad (2.79)$$

where Γ is the spontaneous decay rate from the excited level, c is the speed of light and ϵ_0 is the permittivity of free space.

2.4.1.1. Dipole potential and scattering rate. With the expression for the polarizability of the atomic oscillator we can derive an explicit expression for the dipole potential and scattering rate.

$$\begin{aligned} U_{\text{dip}} &= -\frac{1}{2\epsilon_0 c} \text{Re} \left(6\pi\epsilon_0 c^3 \frac{\Gamma/\omega_0^2}{\omega_0^2 - \omega^2 - i(\omega^3/\omega_0^2)\Gamma} \right) I(\mathbf{r}) \\ &= -\frac{3\pi c^2}{2\omega_0^3} \left(\frac{\Gamma}{\omega_0 - \omega} + \frac{\Gamma}{\omega_0 + \omega} \right) I(\mathbf{r}) \end{aligned} \quad (2.80)$$

$$\begin{aligned} \Gamma_{\text{sc}} &= \frac{1}{\hbar\epsilon_0 c} \text{Im} \left(6\pi\epsilon_0 c^3 \frac{\Gamma/\omega_0^2}{\omega_0^2 - \omega^2 - i(\omega^3/\omega_0^2)\Gamma} \right) I(\mathbf{r}) \\ &= \frac{3\pi c^2}{2\hbar\omega_0^3} \left(\frac{\omega}{\omega_0 - \omega} \right)^3 \left(\frac{\Gamma}{\omega_0 - \omega} + \frac{\Gamma}{\omega_0 + \omega} \right)^2 I(\mathbf{r}) \end{aligned} \quad (2.81)$$

The above expressions are valid for any driving frequency and again show two resonant contributions as in section 2.1.2.1. Using the definition for detuning $\delta \equiv \omega - \omega_0$ and apply the rotating wave approximation the expressions for the dipole potential and scattering rate become

$$U_{\text{dip}}(\mathbf{r}) = \frac{3\pi c^2}{2\omega_0^3} \frac{\Gamma}{\delta} I(\mathbf{r}) \quad (2.82)$$

$$\Gamma_{\text{sc}}(\mathbf{r}) = \frac{3\pi c^2}{2\hbar\omega_0^3} \left(\frac{\Gamma}{\delta} \right)^2 I(\mathbf{r}) \quad (2.83)$$

These equations show two very important features for dipole trapping. First of all there is the dependence on the sign of the detuning. If the laser is detuned below the atomic resonance, $\Delta < 0$, the dipole potential is negative and the interaction attracts atoms into the light which constitutes an attractive interaction. When δ is positive the atom is repelled from regions of high intensity and potential minima correspond to minima in the intensity. Moreover, since the dipole potential is proportional to $I(\mathbf{r})/\Delta$ whereas the scattering rate is proportional to $I(\mathbf{r})/\Delta^2$ requires dipole traps operate at large frequency

detunings $\delta \ll \Gamma$. Working at detunings that are sufficiently large the scattering is reduced while the trap depth remains reasonable [15].

2.4.2. Focused beam traps. Using equation (2.74) and (2.82) we see that the dipole force is given by

$$\mathbf{F}_{\text{dip}}(\mathbf{r}) = -\frac{3\pi c^2}{2\omega_0^3} \frac{\Gamma}{\delta} \nabla I(\mathbf{r}) \quad (2.84)$$

If the frequency of the light field is tuned below the atomic resonance then the dipole force points towards increasing intensity. This means that the focus of a laser beam already constitutes a stable dipole trap for atoms [15].

The simplest way of creating a dipole trap in three dimensions is using a focused Gaussian laser beam tuned below the atomic resonance. The intensity profile of a Gaussian laser beam with power P propagating along the z -axis is given by [15]

$$I(r, z) = \frac{2P}{\pi w_{\text{beam}}^2(z)} e^{-2r^2/w_{\text{beam}}^2(z)} \quad (2.85)$$

where r denotes the radial coordinate and $w_{\text{beam}}(z) = w_{\text{waist}} \left(1 + (z/z_R)^2\right)^{1/2}$ is the $1/e^2$ radius depending on the z coordinate. The minimum radius w_{waist} is called the beam waist and $z_R = \pi w_{\text{waist}}^2/\lambda$ denotes the Rayleigh length. The Rayleigh length is a factor $\pi w_{\text{waist}}/\lambda$ larger than the beam waist which makes the potential in the radial direction much steeper than in the axial direction. Using the intensity distribution one can derive the optical dipole potential using equation (2.82). The maximum intensity is given by

$$I_0 = I(0, 0) = \frac{2P}{\pi w_{\text{waist}}^2} \quad (2.86)$$

which also determines the maximum trap depth. The maximum trap depth is given by filling in this expression into equation (2.82)

$$\begin{aligned} U_{\text{max}} = |U_{\text{dip}}(0, 0)| &= \frac{3\pi c^2}{2\omega_0^3} \frac{\Gamma}{\delta} I(0, 0) \\ &= \frac{3\pi c^2}{2\omega_0^3} \frac{\Gamma}{\delta} \frac{2P}{\pi w_{\text{waist}}^2} \\ &= \frac{3c^2 P}{\omega_0^3 w_{\text{waist}}^2} \frac{\Gamma}{\delta} \end{aligned} \quad (2.87)$$

If the thermal energy of the ensemble is much smaller than the potential depth U_{max} the dipole potential in the center of the trap can be approximated by using 2nd order Taylor expansion [15]

$$U_{\text{dip}} \approx \frac{3\pi c^2}{2\omega_0^3} \frac{\Gamma}{\delta} \frac{2P}{\pi} \left(\frac{1}{w_{\text{waist}}^2} - \frac{z^2}{w_{\text{waist}}^2 z_R^2} - \frac{2r^2}{w_{\text{waist}}^4} + \frac{4r^2 z^2}{w_{\text{waist}}^4 z_R^2} \right) \quad (2.88)$$

Neglecting the last term and rearranging we get

$$U_{\text{dip}} \approx U_{\text{max}} \left(1 - \left(\frac{z}{z_R} \right)^2 - 2 \left(\frac{r}{w_{\text{waist}}} \right)^2 \right) \quad (2.89)$$

The optical potential can be approximated by a cylindrically symmetric harmonic potential [15]. The oscillation frequencies of a trapped atom in this potential are

$$\Omega_r = \sqrt{\frac{4}{mw_{\text{waist}}^2} U_{\text{max}}}$$

in the radial direction and

$$\Omega_z = \sqrt{\frac{2}{mz_R^2} U_{\text{max}}}$$

2.4.3. 1D lattice potential. A lattice potential with tightly confining potential wells can be created by realizing a dipole trap with superimposed counter propagating laser beams. The dipole force is strong in a standing wave of light because the intensity changes from a maximum (at the anti-nodes) to zero (at the nodes) over a distance $\lambda/2$ which results in a high gradient of intensity. Two counter-propagating beams of linearly-polarized light produce an electric field given by

$$\begin{aligned}\mathbf{E}(\mathbf{r}, t) &= \hat{\mathbf{e}}\tilde{E}(\mathbf{r}) \left(e^{-i(\omega t + kz)} + e^{-i(\omega t - kz)} \right) + c.c. \\ &= 2 \cos(kz) \left(\hat{\mathbf{e}}\tilde{E}(\mathbf{r}) e^{-i\omega t} + c.c. \right)\end{aligned}\quad (2.90)$$

This adds a factor of $4 \cos^2(kz)$ to equation (2.82). The dipole potential, in terms of U_{\max} , becomes

$$U_{\text{lattice}} \approx 4 \cos^2(kz) U_{\max} \left(1 - \left(\frac{z}{z_R} \right)^2 - 2 \left(\frac{r}{w_{\text{waist}}} \right)^2 \right)$$

where $k = 2\pi/\lambda$. The trapping along the z -axis is modulated with a period of $\lambda/2$.

2.5. Magnetic trapping and evaporative cooling

There is a wide spread of applications connected with magnetic trapping of neutral atoms. In this case we are interested in the applications that use magnetic trapping to cool down atoms below temperatures that can be reached in the optical molasses. As we saw in the previous section optical traps rely on the induced dipole moment and is often done with near resonant light. However many atoms have ground state magnetic dipole moments that can be used for trapping the atoms magnetically [11]. One of the most intensively studied use of magnetic trapping in the last two decades is the realization of Bose-Einstein condensation.

2.5.1. Magnetic trapping. In order to trap atoms it is necessary to exchange kinetic energy for potential energy in the trapping field. For neutral atoms the potential energy has to be stored as internal atomic energy. One consequence of this requirement is that the atomic energy levels shift as a function of position. Another consideration is that practical traps for ground-state atoms are very shallow compared with thermal energy because the energy shift resulting from realistic magnetic fields are usually smaller than $k_B T$ for $T = 1\text{K}$ [11]. This is the reason that magnetic trapping became widely used after the introduction of laser cooling. The small depth of the magnetic trap also demands an high vacuum in which the atoms are trapped because atoms escape from the trap after collisions with atoms from the background gas.

An atom with magnetic moment $\boldsymbol{\mu}$ can be confined by an inhomogeneous magnetic field due to the interaction between the moment and the field. A magnetic dipole $\boldsymbol{\mu}$ in a magnetic field has energy [10]

$$V = -\boldsymbol{\mu} \cdot \mathbf{B} \quad (2.91)$$

For an atom in the state $|IJFM_F\rangle$ this corresponds to a Zeeman energy of

$$V = g_F \mu_B M_F B \quad (2.92)$$

where g_F is the gyromagnetic ratio and μ_B is the Bohr magneton. The energy of the atom depends on the magnitude of the magnetic field only and does not vary with the direction of \mathbf{B} since the dipole stays aligned with the field [10]. The interaction between the field and the magnetic dipole produces a force given by [11]

$$\mathbf{F} = -\nabla V = \nabla(\boldsymbol{\mu} \cdot \mathbf{B}) \quad (2.93)$$

This force confines atoms that are in a so called low-field-seeking state. These are states in which $g_F M_F > 0$ such that the energy decreases as the atom moves to a position with lower magnetic field. Another problem with these kind of magnetic traps is that atoms that accumulate near the center of

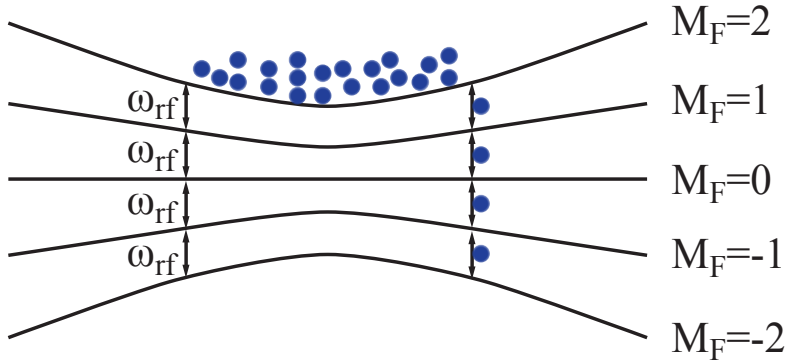


FIGURE 2.9. Atoms in a harmonic trap are evaporatively cooled using radio-frequency radiation to change the state of the atoms to an non-trappable state a certain distance from the center of the trap effectively cooling the atomic cloud.

the trap have very small Zeeman splitting. In this region atoms can transfer from one M_F state to another and be lost to the experiment reducing the lifetime of atoms in the trap. This mechanism is called Majorana spin flipping and can be prevented by adding a bias field [16].

2.5.2. Evaporative cooling. The realization of Bose-Einstein condensation has been an ambition for many years in physics before realizing this goal in 1995. One of the problems with achieving this goal was to first cool down the sample to sufficiently low temperatures and an high enough phase space density. With the techniques of laser cooling it became possible to reach temperatures of μK but in the mid 1990s it became clear that the increase in phase-space density had reached its limit [11]. If the density is too large there is an increase in collision rate and $S + P$ collisions which are generally inelastic is much larger than the $S + S$ collision rate at low temperatures. Since the inelastic energy exchange leads the heating of the atoms, an increasing density results in the loss of cold atoms [11]. So laser cooling alone proved to be insufficient to reach BEC. As it turned out the solution was to use *evaporative cooling* and was used to cool atoms for the first time in 1988 to cool down spin polarized atomic hydrogen. The basics of evaporative cooling are simple. The principle is the same as the cooling in a cup of tea where the steam carries away energy from the cup. So in the case of a magnetic trapped sample where the atoms have a Boltzmann distribution of atoms $\mathcal{N}(E) = \mathcal{N}_0 \exp(-E/k_B T_1)$. We now allow all atoms with an energy $E > E_{\text{cut}}$ to escape and the remaining distribution has less energy per atom after collisions have re-established thermal equilibrium. Repeating this procedure decreases the temperature of the atomic sample. During this evaporation atoms are lost to the trap however, phase-space density increases or at the very least stays the same because the atoms sink lower in the potential when they are cooled down [10]. One particular method of evaporative cooling, which is also used in the experiment described in the next chapter, is to use radio frequency radiation to drive transitions between trapped and untapped states. This technique drives transition between trappable and non-trappable states at a certain distance from the trap center as is shown graphically in figure (2.9). Radiation at frequency ω_{rf} drives the $\Delta M_F = \pm 1$ transition at a radius r that satisfies $g_F \mu_B r \nabla B = \hbar \omega_{rf}$. Hot atoms whose oscillations extend beyond this radius are removed (see figure (2.9)).

2.5.3. Bose-Einstein condensation. One of the main driving forces to develop the techniques of laser cooling and evaporative cooling was to the reach the holy grail of *Bose-Einstein condensation*. Bose-Einstein condensation (BEC) was first predicted by S.N. Bose and A. Einstein [2] To explain the Planck distribution law for black body radiation they developed the Bose-Einstein statistical mechanics of identical particles (bosons), even before the introduction of quantum mechanics and wavefunctions.

The Fermi-Dirac statistic (fermions) came only after the advent of quantum mechanics and the Pauli exclusion principle. The Bose-Einstein distribution is given by

$$N(E) = \frac{1}{e^{\beta(E-\mu)} - 1} \quad (2.94)$$

where $\beta \equiv 1/k_B T$ and μ is the chemical potential. For photons μ vanishes and equation (2.94) is exactly the Planck distribution. The connection with BEC is that Einstein realized that for sufficiently low temperatures the total energy can be minimized by having a discontinuity in the distribution for the population of the ground state [11]. This means that for low enough temperatures the total energy of a sample of atoms would be minimized if there were a significant fraction would avalanche into the ground state, and an infinitesimal fraction of the atoms in each to the discrete excited states. This is only true for bosons that can be in the same quantum state. The condition for BEC in a gas can be expressed in terms of the deBroglie wavelength as

$$n\lambda_{dB}^3 = 2.612 \quad (2.95)$$

where n is the spatial density of atoms and

$$\lambda_{dB} = \sqrt{\frac{2\pi\hbar^2}{mT}} \quad (2.96)$$

where m is the atomic mass and the T temperature. The interpretation of equation (2.95) is that when this parameter becomes of the order 1 quantum statistics start to play a role and for the value given the special phase transition to BEC occurs. The underlying cause for this is that the atomic wavefunctions start to become larger than the mean separation between particles. Although it was predicted even before quantum mechanics was developed a BEC was only first observed in 1995 in a gas of rubidium 87 atoms by the group of E.A. Cornell and C. Wiemann at JILA [17] and a few months later by W. Ketterle at MIT [18] in a gas of sodium atoms. One of the reasons for pursuing the experimental realization of BEC are the unique properties of this state of matter. For atoms in a trap that satisfy (2.95) a significant fraction of the atoms is in lowest bound state and the wavefunction spans a large fraction of the accessible volume. This means that there is long range phase coherence in the system and one can make for example an atomic laser. Also the momentum spread of a BEC is extremely narrow allowing one to study quantum mechanical properties in detail.

2.6. Bragg scattering of cold atoms

The theory that is presented so far in this thesis has been used to explain how atoms can be trapped and cooled down. In this section I would like to describe how the atom light interaction can be used to coherently manipulate cold atoms. Manipulating atoms in the same fashion as we manipulate light with optical elements is called *atom optics* and has been subject of study for a long time. The most interesting cases rely on the deBroglie wave nature of atoms, such as diffraction and interferometry [19]. The subject has seen many advances since the realization of Bose-Einstein condensation, mentioned in the previous section, since this is the ultimate coherent atom source. A BEC provides a collection of atoms all in the same state with an extremely narrow momentum spread. An especially interesting case is combining a BEC with a optical lattice. This setup provides a way of studying quantum systems analogous to electrons in a solid-state crystal however, in this case there is an enormous control over both the lattice and particles [20].

The way cold atoms diffract of a periodic potential is largely dependent on the parameters of the lattice. One regime of scattering that, the focus of this section, is Bragg scattering. Analogous to the way light can Bragg diffract from a thick crystal an atomic beam can Bragg diffract from a standing light wave provided that it interacts with it for a sufficiently long time. In this regime the periodic potential from the standing wave acts as a diffraction grating for the matter wave. In the case of Bragg

scattering light of an atomic crystal the incident light has to satisfy the so called *Bragg condition* for the angle of incidence. The same condition holds for scattering an atomic wave off a periodic potential (figure (2.10b)). Thus Bragg scattering provides a method for deflecting atoms or splitting atomic wave-packets coherently. One consequence of this coherence is interference. In an interferometer atom waves are split into two separate paths and combine again resulting in interference patterns which can be observed and exploited for scientific gain [21]. In our experiment however, we are not dealing with a moving atomic beam but with stationary atoms. In this case the condition for the angle of incidence translates to a condition for the frequency shift between the two laser beams that compose the in this case thus "moving standing" wave. Furthermore the atoms have to interact with the light for a sufficiently long time. In the case of moving atoms this is determined by the "thickness" of the optical grating, for stationary atoms we can control the interaction time by varying the pulse duration. Under these conditions Bragg diffraction can be viewed as a stimulated Raman transition between two momentum states [19].

Optical lattices can be used to study a wide variety of properties of the gas. Depending on the intensity of the laser beams, the detuning from atomic resonance and the time the light interacts with the atoms different regimes of scattering can be entered. First of all the focus of this thesis is the coherent Bragg scattering process. This requires low optical potential and consequently long interaction times to drive transitions. In the opposite the Raman-Nath regime, where atoms scatter into many orders, requires higher light potentials and short interaction times [22, 23]. Another interesting subject of study has been the interactions between atoms using optical lattices. For example one can study the superfluid to Mott-insulator phase transition [8, 24].

In this section we study Bragg scattering process of a stationary BEC in detail. In the first section we derive the Bragg condition for a stationary BEC and in the second section we make an analogy with the Rabi oscillations we encountered in section 2.1.

2.6.1. 2-photon scattering process. *n*th order Bragg diffraction by a moving standing wave can be viewed as a $2n$ -photon stimulated Raman process in which photons from one beam are absorbed and stimulated to emit into the other beam. The scheme for this process is depicted in figure 2.11. The initial and final momentum states from an effective two-level system coupled by the multi-photon Raman process. Starting from figure 2.11a where the atom has initial momentum $\mathbf{P}_{\text{atom}} = \hbar\mathbf{k}_I$ along

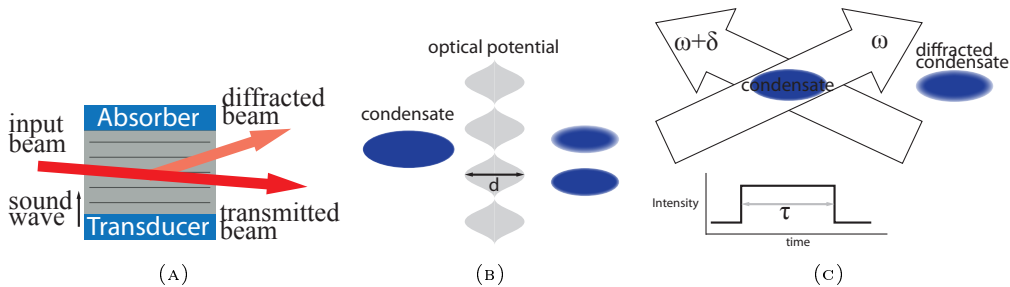


FIGURE 2.10. Bragg scattering of light from a crystal (A) is in essence the same as scattering an atomic wave off a periodic potential formed by a standing wave (B). A stationary cloud of atoms can also be Bragg diffracted only now the pulse duration determines the interaction time apposed to the thickness of the grating and the Bragg condition is given by the frequency detuning between the two counter propagating laser beams (C)

the z -direction⁹ we see that the total initial momentum is

$$\begin{aligned}\mathbf{P}_{\text{initial}} &= \mathbf{P}_{\text{atom}} + \mathbf{P}_{\text{light}} \\ &= \hbar \mathbf{k}_I + \hbar (\mathbf{k}_{L1} + \mathbf{k}_{L2})\end{aligned}\quad (2.97)$$

The resulting magnitude of the momentum is

$$P_{\text{initial}} = \hbar |\mathbf{k}_I| + \hbar \left(\sin\left(\frac{\theta}{2}\right) (|\mathbf{k}_{L2}| - |\mathbf{k}_{L1}|) + \cos\left(\frac{\theta}{2}\right) (|\mathbf{k}_{L1}| + |\mathbf{k}_{L2}|) \right) \quad (2.98)$$

And for the total energy before the interaction we have

$$E_{\text{initial}} = \frac{|\mathbf{P}_{\text{atom}}|^2}{2M} + \hbar (\omega_{L1} + \omega_{L2}) \quad (2.99)$$

What happens next is that the atoms absorbs a photon from the beam incident from the left and is subsequently stimulated to emit into the beam incident from the right (figure 2.11c). For the total momentum in the final state we then obtain

$$\begin{aligned}\mathbf{P}_{\text{final}} &= \mathbf{P}_{\text{atom}} + \mathbf{P}_{\text{light}} \\ &= \hbar \mathbf{k}_f + 2\hbar \mathbf{k}_{L2} \\ &= \hbar \mathbf{k}_I + \hbar (\mathbf{k}_{L1} + \mathbf{k}_{L2}) + 2\hbar \mathbf{k}_{L2}\end{aligned}$$

For the magnitude

$$\begin{aligned}\Rightarrow P_{\text{final}} &= \hbar |\mathbf{k}_I| - \sin\left(\frac{\theta}{2}\right) |\mathbf{k}_{L1}| - \sin\left(\frac{\theta}{2}\right) |\mathbf{k}_{L2}| + \cos\left(\frac{\theta}{2}\right) |\mathbf{k}_{L1}| - \cos\left(\frac{\theta}{2}\right) |\mathbf{k}_{L2}| \\ &\quad + 2\hbar \left(\sin\left(\frac{\theta}{2}\right) + \cos\left(\frac{\theta}{2}\right) \right) |\mathbf{k}_{L2}| \\ \Rightarrow P_{\text{final}} &= \hbar |\mathbf{k}_I| + \hbar \left(\sin\left(\frac{\theta}{2}\right) (|\mathbf{k}_{L2}| - |\mathbf{k}_{L1}|) + \cos\left(\frac{\theta}{2}\right) (|\mathbf{k}_{L1}| + |\mathbf{k}_{L2}|) \right)\end{aligned}\quad (2.100)$$

We can do the same for the total energy after the two photon scattering process

$$E_{\text{final}} = \frac{|\mathbf{P}_{\text{atom}} + \mathbf{P}_{\text{recoil}} + |\mathbf{k}'_{L1}| - |\mathbf{k}'_{L2}||^2}{2M} + 2\hbar\omega_{L2} \quad (2.101)$$

Where \mathbf{P}_{rec} is the recoil momentum the atoms picks up after absorbing and emitting a photon (see also figure (2.11)). If we assume that $|\mathbf{k}_{L1}| \approx |\mathbf{k}_{L2}| = |\mathbf{k}| = k$ equation (2.101) can be written as

$$E_{\text{final}} = \frac{|\mathbf{P}_{\text{atom}}|^2 + |\mathbf{P}_{\text{recoil}}|^2 + 2\mathbf{P}_{\text{atom}} \cdot \mathbf{P}_{\text{recoil}}}{2M} + 2\hbar\omega_{L2} \quad (2.102)$$

where

$$|\mathbf{P}_{\text{rec}}| = 2\hbar k \sin\left(\frac{\theta}{2}\right)$$

where $k = 2\pi/\lambda$ is the wavenumber and λ is the wavelength of the incident light.

Now comparing equation (2.98) and equation (2.100) we see that momentum is conserved in this process as it should be. Furthermore energy should be conserved as well, so by equalizing equation (2.99) and (2.100) we obtain that

$$\hbar (\omega_{L1} - \omega_{L2}) = \frac{|\mathbf{P}_{\text{recoil}}|}{2M} + \frac{\mathbf{P}_{\text{atom}} \cdot \mathbf{P}_{\text{recoil}}}{M} \quad (2.103)$$

This expression can be generalized for $2n$ photon momentum transfers. In this case the equation (2.103) becomes

⁹The calculation can also be done for a initial momentum in any direction

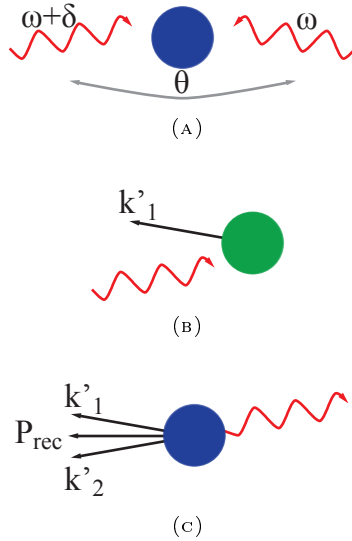


FIGURE 2.11. A representation of a stationary atom absorbing a photon from one beam and stimulated to emit into the other beam causing it to gain momentum. This is not an real representation of the process but it provides an heuristic argument for the $2n$ -photon scattering process.

$$n\hbar\delta_n = \frac{(nP_{\text{recoil}})^2}{2M} + \frac{\mathbf{P}_{\text{atom}} \cdot \mathbf{P}_{\text{recoil}}}{M} \quad (2.104)$$

where $\delta_n = \omega_{L1} - \omega_{L2}$ ¹⁰ is the frequency difference shift between the two lasers and M is the atomic mass. Equation (2.104) allows us to calculate for which δ_n a certain order of Bragg scattering is resonant. The second term in equation (2.104) is the Doppler shift of the resonance and allows the use of Bragg resonances in a velocity-selective way [25].

2.6.2. Rabi oscillations in momentum space. As we have seen in the previous section cold atoms can Bragg diffract off an periodic potential. The initial and final momentum states form an effective two-level system similar to what we have seen in section (2.1)[19]. Analogous to the two level atom the population in the excited momentum state exhibits Rabi oscillations. For the first process the Rabi frequency is derived in appendix E and is given by

$$\Omega_{\text{eff}} \equiv \frac{\Omega^2}{2\delta} \quad (2.105)$$

where Ω is the single photon Rabi frequency of the two level atom from equation (2.13) and δ is the detuning from atomic resonance. This Rabi frequency can also be determined for higher order processes and is given by [23]

$$\Omega_n = \frac{\Omega^{2n}}{2^{2n-1}\delta_1\delta_2\dots\delta_{2n-1}} \quad (2.106)$$

where δ_n are the detunings from resonance as indicated in figure 2.12a. Figure 2.12a is a partial transition diagram for the n th-order Bragg diffraction. The transverse momentum states are displayed in units of $\hbar k$ and the first detunings that enter in equation (2.106) for a n th order scattering process are shown. The convention used here is that an atom starts in a momentum state $n\hbar k$ and after scattering $2n$ photons ends up in state $-n\hbar k$. The momentum states follow a parabolic corresponding

¹⁰There is an intensive use of the symbol δ in this thesis. The symbol δ without any subscript or other indication is used for the detuning from atomic resonance. Any other use of the symbol is indicated by an subscript or index

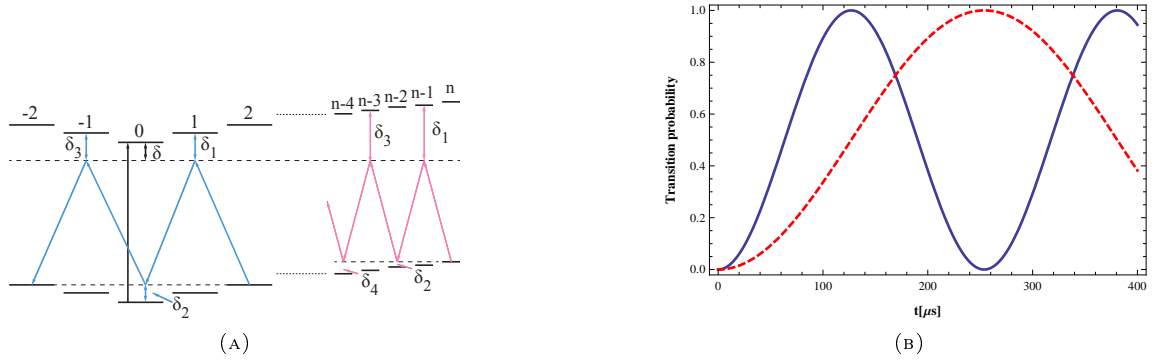


FIGURE 2.12. (A) Partial transition diagram for the 2nd (blue) and n th (red) order Bragg scattering process. The levels are labeled by their transverse momentum states and offset by $n^2\varepsilon$. The transverse momentum is displayed in units of $\hbar k$ and a complete transition is a $2n$ photon process starting in n and ending up in $-n$. The second order Bragg scattering and detunings are indicated in blue. (B) The Rabi oscillations for the first (solid blue) and second order (dashed red) scattering process. We see that the second order Bragg diffraction is a much slower process.

to the $P^2/2M$ kinetic energy [19]. The detunings that enter into equation (2.106) are not all the same and need to be determined separately [23]. For the second order scattering process $\delta_1 = \delta_3 = \delta$ since $\delta \gg \varepsilon$ where $\varepsilon = \hbar k^2/2M$ is the frequency offset associated with one photon recoil and $\delta_2 = 4\varepsilon^{11}$. So this lead to a Rabi-frequency for the second order Bragg scattering process of

$$\Omega_2 = \frac{\Omega^4}{2^3 \delta^2 \cdot 4\varepsilon} \quad (2.107)$$

All the detunings for higher order scattering can be determined and from this a general expression in terms of δ and ε can be obtained [23]

$$\Omega_n = \frac{\Omega^{2n}}{2^{4n-3} ((n-1)!)^2 \delta^n \varepsilon^{n-1}} \quad (2.108)$$

Figure (2.12b) shows the first and second Rabi oscillations for an equal set of parameters. From this picture we see, and also looking at equation (2.108), that in order to drive the second order process one either needs long radiation times or higher powers¹².

¹¹ $\delta_1 = 2\varepsilon!$

¹²There are limits to what high powers means in this case. Since equation (2.108) is derived using a perturbative approach it no longer holds when the intensity becomes to large and the approach breaks down. In this case one enters the Raman-Nath regime and atoms scatter into many orders.

CHAPTER 3

The experimental setup

This chapter will introduce and describe the experimental setup that was used for doing the experiments presented in this thesis. The experimental setup can be divided into two parts. The first part of the setup which was already in place is the "main" experiment called the *Celsius experiment*. The Celsius experiment is the name of the system in which the cold atoms are created and is described in the first part of this chapter. The second part of the experimental setup was built for the purposes of this thesis. We have built a laser setup which allows us to implement a standing wave potential on the cold atoms. The experimental setup of these lasers and its capabilities together with the expected experimental results are described in the second section of this chapter.

3.1. The Celsius experiment

The Celsius experiment stands for Chip Experiment for Low-dimensional Strongly Interacting Ultra-cold Systems and was initiated in 2002 at the University of Amsterdam (UvA). The most innovative part of this system is that it uses an *atom-chip* to magnetically trap and evaporatively cool rubidium atoms. One of the focuses at the Celsius experiment is low-dimensional quantum-degeneracy which can be reached by using atom chips. However, this is not the focus of this thesis but since the chip plays a major role in the cooling mechanism we give a short introduction on how the atom-chip works and what the advantages are of using atom chips to do cold atom experiments. After this the experimental steps to reach BEC at the Celsius experiment is discussed.

3.1.1. Atom-chip experiments. The core of the Celsius experiment is formed by the micro-trap for cold atoms, the atom chip shown in figure 3.1a . The trap basically consists of three layers of current-carrying wires. The perhaps most interesting layer is the surface layer which consists of a silicon substrate coated with a patterned gold layer. In this gold layer parts are etched away creating a number of wires in a certain pattern, figure 3.1b. Beneath the surface layer (or above in the actual experiment) there are two layers containing three parallel copper wires each in the x and y -direction respectively which are called miniwires [5]. By sending current through these wires a magnetic field is produced that can be used to trap atoms. The most simple form of such a trap is illustrated in figure 3.2a . The trap illustrated in this figure consists of just one current carrying wire and a bias field B_{bias} (that can easily be created by coils) and creates a tube-like atom trap. If we take the chip in the xy -plane and a current through the miniwire in the x -direction and B_{bias} along y -direction, a trap is created at distance z_0 from the chip. This position and the magnetic field gradient at that point are given by Biot-Savart and can be written as [5]

$$z_0 = \frac{\mu_0 I}{2\pi B_{\text{bias}}} \quad (3.1)$$

$$\frac{\partial B}{\partial z} = \frac{\mu_0 I}{2\pi z^2} \quad (3.2)$$

where μ_0 is the permeability of free space. For a current of 2 A and a bias field of 40 G the trap is 100 μm away from the chip and the gradient is 4 kG/cm [5]. The possibility of creating strong confining traps with modest currents combined with scale reduction and reproducibility make atoms chips experiments

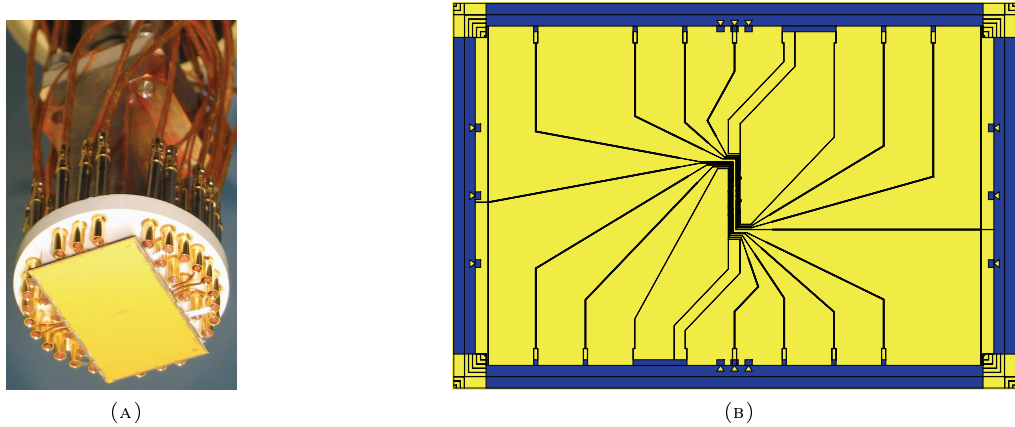


FIGURE 3.1. (A) A picture of the gold surface and the mount of the atom chip. (B) Lay-out of the wire pattern of the atom chip. From the gold surface of the atom chip small lines are etched away leaving an effective pattern of wires. The design of the chip determines what kind of magnetic field you can create using one or more wires. One of the most important wires on the chip is the z-shaped wire which is the largest and runs through the middle. This wire can be used to create a trapping potential in all directions.

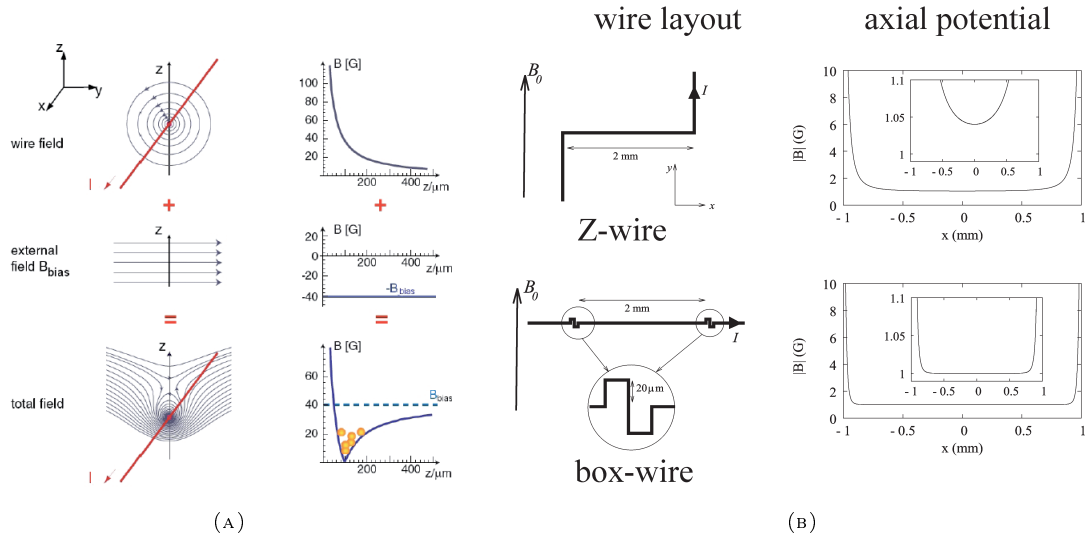


FIGURE 3.2. (A) In the top figure: the magnetic field of a current carrying wire. It curls around the wire and decreases as a function of the distance from the wire. In the middle a constant bias field which is pointed in the z -direction. Bottom figure: the combined magnetic field of a wire and a bias field. This constitutes a tube-like magnetic trap for atoms in this example at $100 \mu\text{m}$ from the wire. Figure taken from [5] (B) Top figure: the magnetic field generated by a z-shaped wire. This configuration constitutes a trap in all directions and is approximately harmonic at the center of the trap in the x -direction. Wires that have little wiggles constitute a more advanced trap. The wiggles also generate confinement in the x -direction but with a much steeper slope. Effectively these wires create a box-like potential for atoms which is a very interesting case to study.

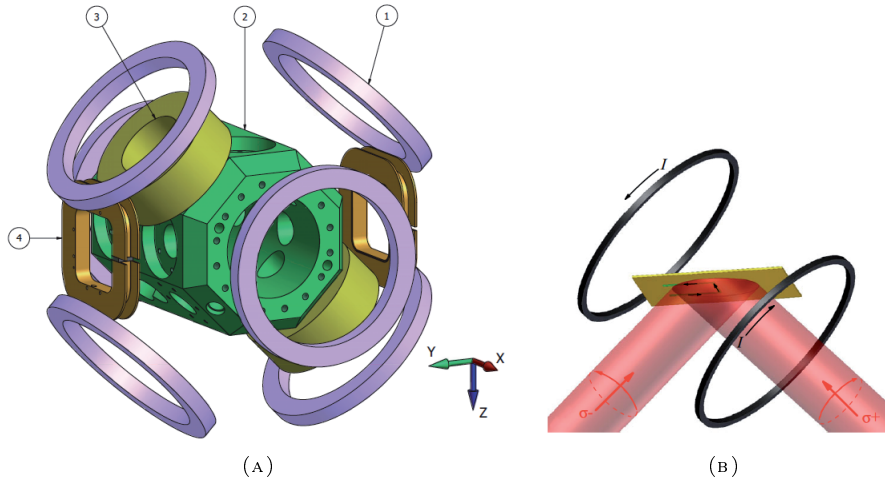


FIGURE 3.3. (A) Schematic figure of the vacuum chamber of the Celsius experiment. The main vacuum chamber is octagonal and is depicted in green and by number 2. The purple coils indicated by number 1 are the compensation coils. These coils are used to generate magnetic fields to compensate for any stray fields. The big yellow coils (number 3) are the MOT coils and are water cooled. The square coils depicted by number 4 are the bias coils and are used to create bias field to magnetically trap atoms using the atom chip. Both figures were taken from [6]. (B) Image of the mirror mot. Two beams with opposite polarization are retro-reflected on the atom-chip and the MOT coils are indicated by the black bands (figure from [5]).

extremely useful [5]. Furthermore the tight magnetic confinement shortens the experimental cycle time and reduces the demands on the vacuum. Finally and perhaps the most useful feature of atoms chips is the possibility to design elaborate potentials [6]. This can be achieved by designing the wire pattern on the gold surface layer in a specific way (figure 3.1b). One way to confine the atoms in all direction is to use the "z-wire" geometry or make an box-like potential using the "wiggled" wires as depicted in figure 3.2b.

3.1.2. The Celsius experiment. The complete setup including all technical detail for the Celsius experiment is described in [5] and [6]. Here we give an overview of the most important elements and the experimental sequence for reaching Bose-Einstein condensation. The main vacuum chamber and magnetic-field coils are depicted in figure 3.3a with the chip and rubidium dispensers inside. The first step is to collect the atoms that are released from the rubidium dispenser in a MOT. Since there is no optical access from all six directions due to the placement of the chip, a *mirror-MOT* is used. The working principle is exactly the same as described in section 2.3.3 but in this case one of the beams is reflected on the surface of the chip (figure 3.3b). The next step is to load the atoms from the mirror-MOT into a *miniwire-MOT* trap where the magnetic field is generated by the chip with wire configuration as shown in figure 3.4 . The laser light for the MOT stage is provided by Toptica DL-100 lasers and sent through a tapered amplifier and is red detuned with 2.7Γ from the $F = 2 \rightarrow F = 3$ of the $5^2S_{1/2} \rightarrow 5^2P_{3/2}$ cycling transition [5]. This is also called the D2-line and is the strongest closed cycling transition in rubidium.

Due to the radiative selection rules some atoms decay to the $5^2S_{1/2}, F = 1$ state and become "dark". These atoms are pumped by the repump laser that is locked on the $F_{S_{1/2}} = 1 \rightarrow F_{P_{1/2}} = 2$ transition such that the atoms can decay to the $5^2S_{1/2}, F = 2$ state and be used for experiment. See figure 3.5 for a scheme of all the optical transitions to which the lasers are locked . After this stage

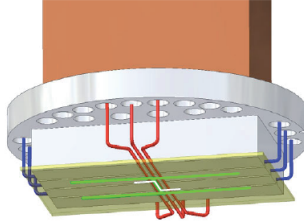


FIGURE 3.4. In green the lay-out of the wires used to create the magnetic for the wire-MOT stage.

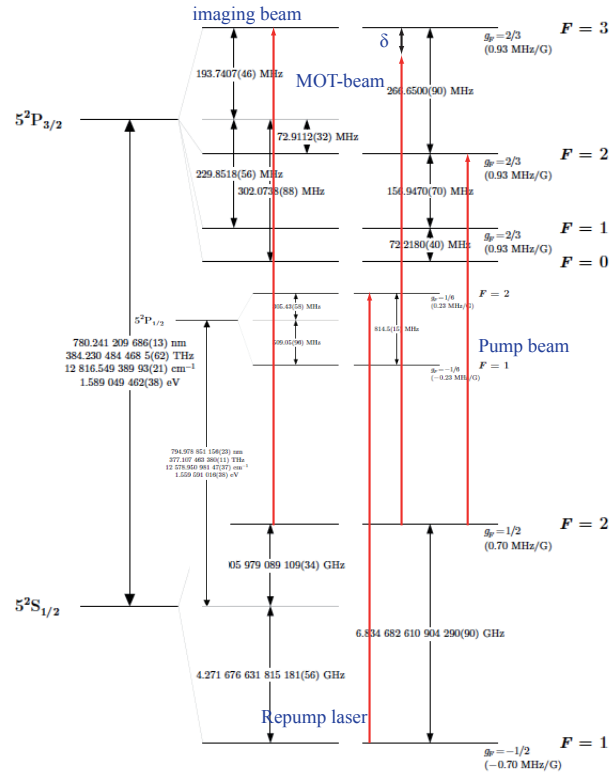


FIGURE 3.5. Figure of the rubidium 87 D2 and D1 transition hyperfine structure. The red lines indicate the lasers frequencies that we use to cool down the atoms. The MOT-beam is detuned from the $F = 2 \rightarrow F = 3$ transition. The repump laser ensures that the $F = 1$ state stays depleted such that all atoms can be used for the experiment and the Pump-beam optically pumps all the atoms to the $M_F = 2$ state using the radiative selection rules. The pump is σ_+ polarized.

the atoms are cooled down to approximately $200\text{ }\mu\text{K}$. The next step in the cooling procedure is to cool down the atoms in the optical molasses as described in section 2.3.2 and temperatures of around $30\text{ }\mu\text{K}$ are reached. The atoms are then optically pumped into the $M_F = 2$ state and trapped magnetically by the miniwires on the atom chip. Finally the atoms are cooled down to quantum degeneracy using evaporative cooling and radio-frequency induced spin flips [5].

3.1.2.1. *Imaging.* The final step in the experimental setup is the acquisition of data. The imaging of the atoms is based on the absorption imaging technique. A full and detailed description of the setup and imaging system is given in [5]. The idea is to illuminate the atomic sample with resonant or near resonant light (figure 3.5) and to record the shadow of the sample on a position sensitive detector such as a CCD-camera. The atoms absorb photons from the probe beam that is traveling in the y -direction (figure 3.6) and emit in all directions. This casts a shadow on the CCD-camera. From this image one can estimate the atomic density of the cloud [26]. The light that hits the atomic sample follows Beers's law for radiation propagating through an absorptive medium, in the y -direction given by

$$\frac{dI(x, y, z)}{dy} = -n(x, y, z) I(x, y, z) \sigma \quad (3.3)$$

where $n(x, y, z)$ is the atomic density, $I(x, y, z)$ is the intensity of the light and σ is the cross-section for an atom absorbing a photon. Integration of equation (3.3) in the y -direction gives the intensity on the detector as

$$I(x, y) = I_0(x, z) e^{-D(x, z)\sigma} \quad (3.4)$$

where $I_0(x, z)$ is the laser intensity before the interaction and $D(x, z)$ is the integrated “2D-density”. The factor $D(x, z)\sigma$ is called the optical density $\mathcal{O}(x, z)$ and can be directly measured by first taking an image with the shadow of the atomic cloud $\mathcal{A}(x, z)$. Then after the atoms have fallen down or have been blown away by the laser beam we take another picture of the beam profile $\mathcal{B}(x, z)$ and finally we take a picture in the absence of light to record the camera noise $N(x, z)$. From this the intensity on the camera and the initial intensity are

$$I(x, z) = \mathcal{A}(x, z) - N(x, z) \quad (3.5a)$$

$$I_0(x, z) = \mathcal{B}(x, z) - N(x, z) \quad (3.5b)$$

Now from equation (3.4) one can write the optical density as

$$\mathcal{O}(x, z) = \ln \left(\frac{\mathcal{B}(x, z) - N(x, z)}{\mathcal{A}(x, z) - N(x, z)} \right) \quad (3.6)$$

The total number of atoms is given by

$$\mathcal{N} = \iint_{-\infty}^{\infty} dx dz D(x, z) = \frac{1}{\sigma} \iint_{-\infty}^{\infty} dx dz \mathcal{O}(x, z) \quad (3.7)$$

There are two ways of calculating this integral. The first one is by counting pixels and converting the integral to a sum

$$\frac{1}{\sigma} \iint_{-\infty}^{\infty} dx dz \mathcal{O}(x, z) \rightarrow \frac{\text{pixel area}}{\sigma} \sum_{\text{all pixels}} \mathcal{O}_{\text{pixel}} \quad (3.8)$$

or by assuming a density distribution (for example Gaussian for an thermal cloud) and fit a suitable density profile to the experimental data. It is also possible to determine the temperature of a thermal cloud by releasing the atoms from the trap and taking pictures for various expansion times. From the expansion speed one can determine the initial velocity distribution and therefore the temperature [13].

3.2. Bragg lasers

Once a gas of cold atoms is produced as described in the previous section one is able to study quantum mechanical properties of the atoms. In this section we describe the experimental setup that was designed for this purpose. We start from the general idea of using two counter propagating laser beams to produce a standing wave of light to manipulate the atoms. This is a very general idea for an

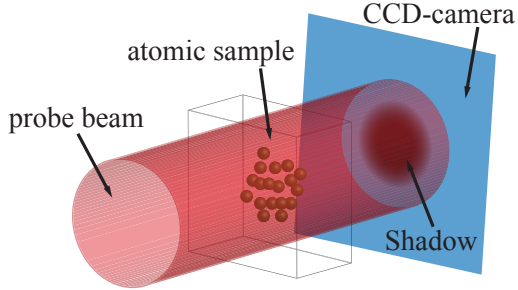


FIGURE 3.6. The idea of absorption imaging. The atomic sample absorbs light from an incoming laser beam of intensity I_0 and emits in all directions. The result is a shadow on the CCD camera at the position of the atomic cloud. From this shadow one can determine for example number of atoms and the temperature of the atoms.

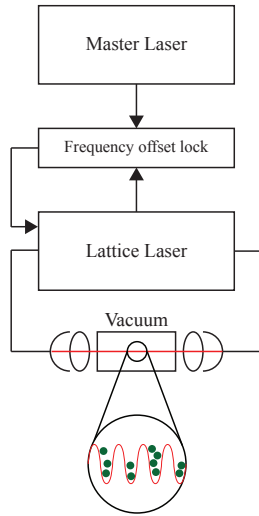


FIGURE 3.7. General schematic overview of the experimental setup to perturb atoms in a vacuum chamber with a standing wave. The master laser is locked to an atomic transition and used as a reference frequency for the lattice laser. The lattice laser is detuned from atomic resonance and stabilized using a frequency offset lock. Subsequently the light from the lattice laser is manipulated such that two beams emerge that constitute the standing wave.

experimental setup which allows versatile experiments however, full control of the light field is needed to be able to enter all regimes. To get a high level of control over the light field is challenging and not straightforward. Thus from this widespread idea we describe the design considerations of our laser setup and discuss the possibilities and deficiencies that this leads to. In the final part of this section we propose a specific experiment that can be done with this setup and we comment on what the expected results are based on the theory that we developed in the first chapter.

3.2.1. Laser setup. The initial idea was to build two lasers to produce the required light field that interacts with the atoms as depicted in figure 3.7. To avoid spontaneous emission the frequency with which we perturb the atoms has to be detuned from atomic resonance, in this case the $5^2S_{1/2} \rightarrow 5^2P_{3/2}$ or D2 hyperfine transition in rubidium 87. Since we want to control the amount of detuning from atomic resonance we developed the following scheme. We build a laser which is called *Master laser* that was locked on the $F = 2$ to $F = 3$ D2 hyperfine transition of rubidium 87. This frequency

stabilized laser was used as a reference frequency for the *Lattice laser* which was used to produce the light that would be used for doing experiments. A detailed description of the setup of the master laser is given in section 3.2.1.1. The setup for the lattice laser is more comprehensive in order to have a more extensive control of the light and is described in detail in section 3.2.1.2.

3.2.1.1. Master laser. The main purpose of this laser is to provide a stable reference frequency for the lattice laser. Since we want to control the amount of detuning from atomic resonance we want to stabilize the frequency of the master laser on the atomic transition. For this purpose a Doppler free spectroscopy unit of Rubidium 87 gas was build to lock the laser on the D2 transition.

The schematic setup for the master laser is shown in figure 3.8a. The light is produced by a temperature stabilized external cavity diode laser. A Sanyo DL-7140-201 laser diode with a nominal wavelength of 780 nm was mounted on a thermoelectric stabilized base in a Littrow configuration, figure 3.8b. The output of the diode was aimed at a diffraction grating which was mounted on a piezo element such that the external cavity length can be controlled. The temperature, diode current and piezo voltage are controlled by respectively Toptica Temperature Control TC-110, Current Control CC-110 and Scan Control SC-110 units mounted in a Toptica DL-110 laser rack. Both diode current and piezo voltage are scanned simultaneously to maximize the mode-hop free frequency range. Furthermore the current is modulated with by 20 MHz to perform frequency-modulated spectroscopy. The light is then passed through an $\lambda/2$ -waveplate and a polarizing beam splitter. The deflected part of the beam which intensity is determined by the setting of the waveplate is passed through a glass cell containing Rubidium gas and retro-reflected back into the cell by a mirror after going through a $\lambda/4$ -waveplate. This ensures that the polarization is turned over $\pi/2$ and all the light goes through the polarizing beam splitter and is detected by a Thorlabs PDA 10A-EC photo-detector. The spectrum recorded by the photo-detector is a Doppler-saturated absorption spectrum and it resolves the hyperfine structure of the atomic transition in Rubidium 87. The signal of the photo diode is supplied to an Toptica Pound Drever Hall Detector PDD-110 which basically demodulates the signal and generates the derivative of the spectrum. Instead of showing absorption peaks at the atomic transitions the spectrum now consists of steep slopes at transition energies. This signal can be used by an Toptica PID-regulator

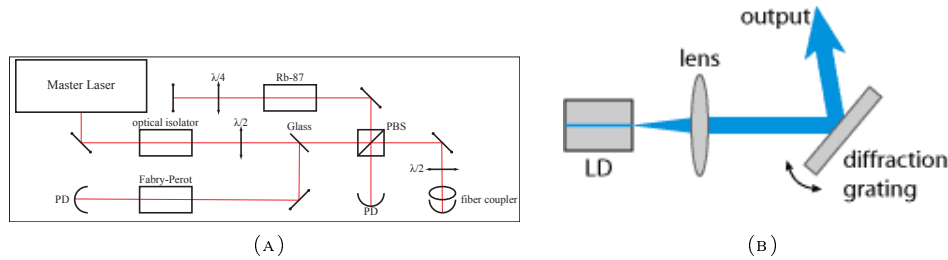


FIGURE 3.8. (a) Schematic overview of the master laser. The light is produced by a laser diode with frequency around 780 nm. A Doppler saturated spectroscopy signal is generated by passing the light twice through a cell containing rubidium 87 vapor. This signal is used to lock the laser on an atomic transition. The frequency stabilized light is coupled into a fiber and used to send to the frequency offset lock of the lattice laser. (b) The inner part of the external cavity laser. The laser diode is mounted in a Littrow configuration. The angle of the grating is controlled by the voltage over the piezo which also controls the length of the external cavity and the feedback to the laser diode. Diode current and piezo-voltage are scanned simultaneously to maximize single mode operation.

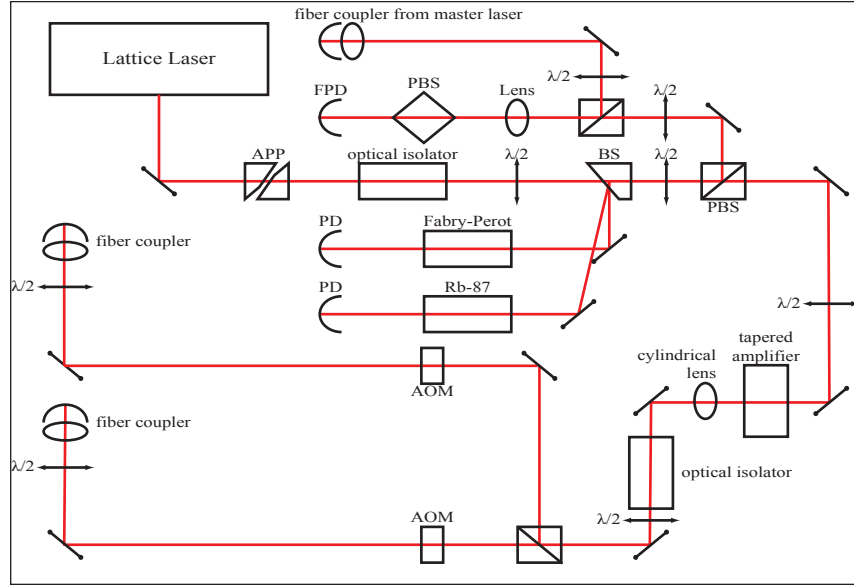


FIGURE 3.9. Schematic representation of the lattice laser. After the first polarizing beam splitter the light that reflects is overlapped with the light from the master laser. The beat signal is used to create the frequency offset lock. The stabilized light is fed into an tapered amplifier to increase power. The light is then split and guided through two two AOM's. The first diffracted order is coupled into two polarization maintaining fibers and used to carry out the experiment.

PID-110 to actively stabilize the output frequency of the diode at the Rubidium D2 transition. In addition a piece of glass is placed in the path of the laser beam to tap off a small amount of light which is directed into a home build Fabry-Perot. This in order to ensure single mode operation of the laser.

The light from the original beam that passes straight through the polarizing beam splitter is coupled into a fiber. This light is overlapped with the light from the lattice laser in order to create the frequency-offset-lock.

3.2.1.2. Lattice laser. The design of the lattice laser is somewhat more complicated than the design for the master laser due to the fact that there are more requirements for the light field that perturbs the atoms. The schematic overview of the beam path is given in figure 3.9. The laser diode is the same one that was used to provide the light for the master laser. The beam profile of such lasers is somewhat elliptical so an anamorphic prism-pair is inserted into the beam path to obtain a more Gaussian profile of the beam. The optical isolator is again to prevent feedback from the optical elements to the laser diode. After the optical isolator the beam is guided through a beam sampler. The two deflected beams are inserted into a Fabry-Perot to check single mode operation and passed through a rubidium 87 spectroscopy cell as an overall check of the frequency range of the diode. After the beam sampler the light is split and the part that is deflected by the polarizing beam splitter is overlapped with the light that was coupled into a fiber from the master laser. The overlapped beams are focused on a Hamamatsu G4176-03 fast-photo-detector which is able to record the beat signal between the two laser beams. This signal is used for the frequency offset lock.

The frequency offset lock basically consists of an electric circuit that compares two frequencies and generates an error signal that can be used for locking. In this case "one" frequency is provided by the beat signal recorded by the fast photo diode. This signal is amplified by three Mini-Circuit [model] amplifiers and divided by 32. The *set* frequency is provided by a Mini-Circuit [model] voltage

controlled oscillator set at 80 MHz realizing a detuning of 2.5 GHz. The line width of the lattice laser when it is locked is about 6 MHz which should be narrow enough to observe Bragg scattering.

The light that goes straight through the beam splitter is fed into a tapered amplifier. This is an important element of the optical setup since it (as the name already suggests) amplifies the light and it is a limiting factor in the maximum intensity we can obtain. We use a GaAs TPA0780 tapered amplifier and the casing is home build. The temperature of the tapered amplifier is controlled by a Topica TC-110 and set at 23 C°. The maximum current supplied to the tapered amplifier is 2 A and is supplied by a home build power supply. The characteristics of the tapered amplifier are shown in figure 3.10 . The tapered amplifier is usually seeded with about 20 mW of seeding power which results in a maximum of a little more than 1 W output power. One common problem with these kind of amplifiers is that the beam profile gets distorted. This becomes a problem later when the light has to be coupled into an fiber which requires, for high coupling efficiency, a perfect Gaussian beam profile. After the tapered amplifier there is another optical isolator to prevent back reflection onto the amplifier because this can damage the amplifier especially at these high powers.

After the second optical isolator the light is split using a 50/50-cube or non-polarizing beam splitter. Each of this beams is guided through an *acousto optic modulator* (AOM) after which the beams are coupled into fibers. The AOM's perform a crucial role in this setup so we give a short explanation on how they work and why we use them. An AOM uses the acousto-optical effect to diffract and shift the frequency of a light beam using sound waves. A piezoelectric transducer driven by an oscillating electric oscillator is attached to a crystal which creates sound waves in the crystal, figure 3.11. These sound waves modulate the index of refraction in a periodic way. The incoming light scatters off this periodic index modulation and results in interference, in the same way light can Bragg diffract off a crystal structure.

The use of AOM's allows us to manipulate the light in a couple of aspects. The first thing one can control is the deflection of the light. Incident light scatters under an angle θ depending on the wavelength of the light and the frequency of the modulation. If the incoming light satisfies the *Bragg angle* deflection in only the first order can be achieved with efficiencies up to 80%. Another feature that the AOM's provide is the control of intensity. The intensity of light scattered into the first order

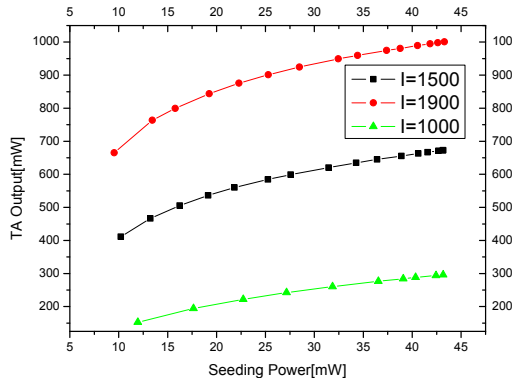


FIGURE 3.10. Characteristics of the tapered amplifier. The intensity of the light saturates for higher seeding powers. The maximum current at which we can drive the tapered amplifier is 2 A which gives a maximum output power over 1 W.

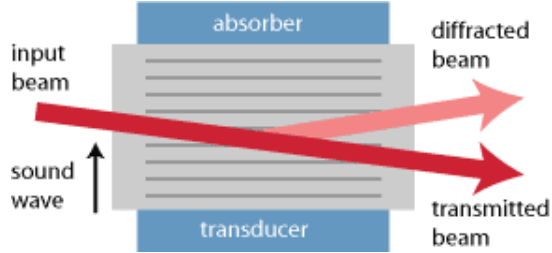


FIGURE 3.11. Basic configuration of an AOM. The light incident from the left is scattered off the sound waves generated by the piezo-electric transducer. A part of the light is scattered into the first order if the incident beam satisfies the Bragg condition. Under the right conditions scattering efficiency of up to 85% into the first order can be reached.

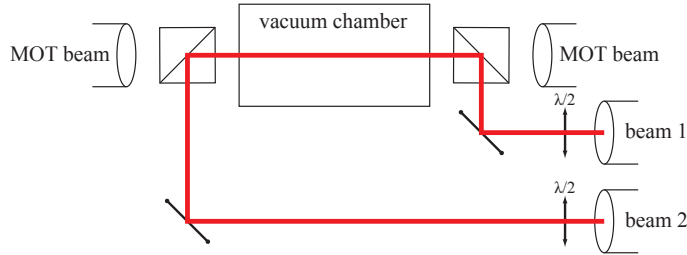


FIGURE 3.12. Experimental setup on the vacuum chamber. The polarizers are chosen such that the polarization of the light is vertical. The cubes in front of the vacuum chamber are 50/50 cubes which causes a 50 % loss in intensity but they are necessary to overlap the light with the MOT-beams

can be controlled by the intensity of the sound waves in the crystal. Together the control of diffraction and intensity allow us to make a pulsed laser where we control the intensity of the pulse¹.

A pulsed laser could also be created by using mechanical equipment however, the switching of light is much faster using this method which is desired for Bragg scattering. As mentioned before the AOM also shifts the frequency of the light by an amount equal to the frequency of the sound waves. In some cases this shift has to be taken into account or can be used on purpose. In our case we use Crystal technology 3080-122 AOM's and in optimal conditions we can achieve up to 83% diffraction efficiency.

Finally the light is coupled into Schäfter-Kirchhof PMC780-4 polarization maintaining fibers. At maximum power AOM-1 (see figure 3.9) has a coupling efficiency of 27% and AOM-2 an efficiency of 39%. The low coupling efficiency in AOM-1 is due to the distorted beam profile after the tapered amplifier. Since the beam paths are not equal the efficiency of AOM-2 is higher. All of this results in a maximum power of respectively 61 mW and 91 mW after the fibers.

3.2.1.3. Implementation on the Celsius experiment. The final experimental preparations before the experiments could be carried out is to implement the lattice laser on the Celsius experiment. The main setup is depicted in figure (3.12). Each of the optical fibers is coupled into a Schäfter+Kirchhoff 60FC-T-4-M100S-37 fiber collimator. To ensure that the axes of the linear polarized light after the polarization maintaining fibers matches a $\lambda/2$ -waveplate is inserted after the fiber and rotated such

¹This is to our knowledge the only way to realize a frequency shift in the range of $\approx 1\text{ kHz}$ between two lasers with a line width of 6 MHz.

that both axes are vertical. The beams are overlapped with the center as close as possible to the surface of the chip.

3.2.2. Expected results. The first experiment that we were looking to do is to Bragg diffract the atom cloud into the first order completely. As we have seen in section 2.6 the atoms undergo Rabi-oscillations between the different momentum states. From equation (2.104) we can calculate the frequency difference between the two Bragg lasers first order Bragg scattering is resonant. If we take the angle between the beams to be $\theta = 180^\circ$ and $n = 1$ equation (2.104) becomes

$$\begin{aligned}\hbar\delta_1 &= \frac{(2\hbar k)^2}{2M} \\ \Rightarrow \delta_1 &= \frac{2\hbar k^2}{M}\end{aligned}\quad (3.9)$$

where \hbar is the reduced Planck's constant, $k = 2\pi/\lambda_{D2}$ where λ_{D2} is the wavelength of the D2-transition of rubidium light and M is the atomic mass which are all given in table (A.1). For these conditions first order Bragg scattering is resonant at

$$\frac{\delta_1}{2\pi} = 15.083 \text{ kHz} \quad (3.10)$$

Furthermore, the oscillation period is given by equation (2.22) with Ω replaced by Ω_{eff} given in equation (E.10). If we combine equation (2.13), (E.10) and equation (2.22) we can write the population in the first excited momentum state as

$$|c_{|G,2\hbar k\rangle}|^2 = \sin^2 \left(\frac{(eX_{EG})^2 |\mathbf{E}_0|^2}{4\delta\hbar^2} t \right) \quad (3.11)$$

where $eX_{EG} = \mu$ is the matrix transition element for the rubidium D2 transition and $|\mathbf{E}_0|^2$ is related to the intensity of the light beams through equation (2.72) which is again related to the total power of the beam through equation (2.86). This means that the oscillation period is dependent on the amount of power in the beams, the waist size of the beam and the detuning δ from atomic resonance. We now poses all the elements needed to calculate a for example a π -pulse. The value matrix element μ is listed in table A.1 and for the following set of conditions a π -pulse has a duration of ²

$$\left. \begin{array}{l} P = 30 \text{ mW} \\ \delta = 3 \cdot 10^9 \text{ Hz} \\ w_{\text{waist}} = 0.9 \text{ cm} \end{array} \right\} \tau_\pi = 69.25 \mu\text{s} \quad (3.12)$$

In this time the atoms fall under the influence of gravity $305.4 \mu\text{m}$. The choice of τ_π is a trade off between the time resolution of the computer that drives the AOM's and the falling time in gravity. The time that the atoms fall under gravity is preferred to be short so that the atoms don't feel large fluctuations in the light field but has to be long enough to get a good resolution. For these conditions figure 3.13 show the plot of the first two Rabi oscillations of the first order Bragg scattering (blue line). Also in the same figure are plots for when the lasers are not tuned on Bragg resonance which leads to lower transition rates. This detuning from Bragg resonance enters into equation (3.11) the same as the detuning from atomic resonance appears in equation (2.21). These simulations do not take into account any damping factors such as collisions with the background gas.

²Note that in equation (3.12) δ is not an angular frequency and in the convention of equation (3.11) it is so before computing the length of a π -pulse this number has to be multiplied by 2π .

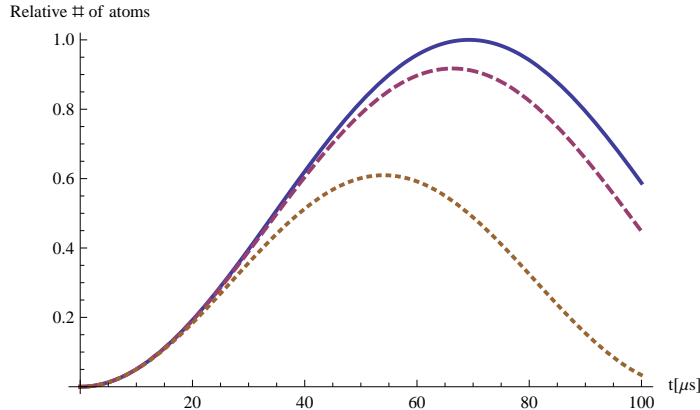


FIGURE 3.13. A plot of the time evolution of the population in the first order diffracted state. This plot was calculated for a total beam power of 30 mW, a beam radius of 0.9 cm and a detuning from atomic resonance of 3 GHz from atomic resonance. The solid blue line is a plot for the Rabi oscillations with zero detuning from Bragg resonance. From this we can see that the duration of a π -pulse is $69.25 \mu\text{s}$. The dashed red line and the dotted brown line are the Rabi-oscillations when the frequency shift δ_n between the two Bragg lasers does not exactly match the Bragg condition. In this case we see that the transition amplitude goes down and the oscillation period goes down.

CHAPTER 4

Results

We finally arrived at perhaps the most interesting chapter: the results. It might at this point be worthy to comment on some of the problems that we encountered during the experiments. This project was setup to take about ten months of which approximately half the time was reserved for building the setup and doing the calculations and the other half for doing experiments and writing this thesis. However, experimental physics is arguably the most unpredictable of all professions in science. Right at the point where we were ready to start doing experiments an accident happened that destroyed our atom chip requiring it to be replaced. The cause of the accident was an uncontrolled current flow through the rubidium dispensers. The result of this was very high rubidium pressure estimated to be around 10^{-6} mbar and we clearly observed fluorescence in the vacuum chamber. As an effect of this the color of the atom-chip changed from gold to gray and the reflectivity of the chip was reduced from 95 % to 20 %. We suspected that due to the high rubidium pressure rubidium has migrated into the gold surface layer of the chip destroying the reflectivity. In order to rescue the chip we backed the chip at 180 °C without any result. We suspect that the AuRb alloy formed on the chip cannot be removed at temperatures below 480 °C. As a result of this accident the atom-chip had to be replaced. To avoid such an accident to happen in the future we installed a 12 A fuse in series with a solid state relais that is triggered by a voltage comparator. The comparator compares an adjustable set voltage with a monitor voltage from the pressure gauge. In our system we have set the solid state relais to switch the current through the dispenser off if the pressure raises above 10^{-8} mbar. Due to this "normal" complication there was only little time left to do experiments and to analyze the data. All the data that is presented in this chapter has been gathered and analyzed in course of about two and a half weeks.

The chapter starts with a description of how the data was analyzed. Subsequently the most important results for the Bragg diffraction experiments are presented. In the final section, to show the versatility of the setup, we demonstrate a different scattering process namely Raman-Nath scattering.

4.1. Analyzing data

As already mentioned in section 3.1.2.1 the type of data that we have to analyze are absorption images. The Labview program that controls the experiment sets the CCD camera to take three pictures in each experimental cycle. It takes an image with atoms, with only light and with no light. From these three images the absorption image is created [5]. This absorption image is then saved as a matrix of numbers and imported into Mathematica 7.1 for further analysis.

Some typical images that we need to analyze are shown in figure 4.1b where the color scale is given in figure 4.1a. Figure 4.1b shows four of the most characteristic results of the experiment. In the top left figure we see a condensate in the middle with no atoms diffracted to either the right or the left. This picture was taken for a Bragg pulse where the frequency shift of the Bragg beams was set to $\delta_n = 0$ kHz. The fringes that we observe on the sides are probably due to optical interferences caused by the sharp edges of the almost one dimensional condensate. In the bottom left picture we see a condensate in the middle and atoms that are diffracted to the right. This picture corresponds to

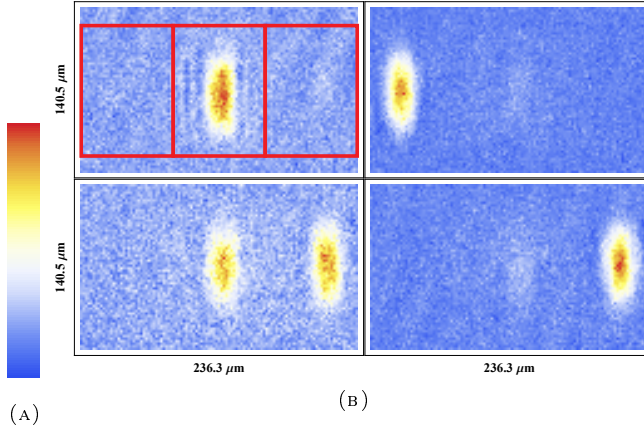


FIGURE 4.1. (a) The color scale for the figures in b. The color scale runs from blue, low atom number, to red, high atom number. (b) Example absorption images of a non resonant pulse (top left) a $\pi/2$ -pulse (bottom left) and a π -pulse to the left and right respectively. The three red boxes in the top left figure each represent a diffraction order $(-1,0,1)$ respectively.

a $\pi/2$ -pulse where the frequency shift is set to resonance ($\delta_n = 15$ kHz). The two figures on the right correspond to a π -pulse to the right and to the left respectively.

The method that we used to analyze the data is quite straightforward. Since we are interested in the transition probability we need to know the relative number of atoms that gets diffracted which is given by

$$\text{transition probability} = \frac{N_{\text{left}} + N_{\text{right}}}{N_{\text{total}}} \quad (4.1)$$

The way to determine these numbers is illustrated in the top left picture of figure 4.1b. There are three red boxes drawn each corresponding to a order of diffraction $-1, 0$ and 1 respectively. To calculate the total number of atoms we add the pixel values of all three boxed in the horizontal direction to obtain a profile. This profile we fit with a Gaussian function and integrate this function to obtain a relative total atom number¹. We now do the same procedure but for the left and right box alone to obtain the relative number of atoms that is diffracted. The error on the calculation of the number of atoms is calculated by the error on the fitting parameters of the Gaussian function. The total error on the transition probability is composed of the error given by the fitting parameters and, if multiple measurements were done for one data point, the statistical error.

4.2. Rabi oscillations

At the beginning of chapter 2 we showed that a driven two level system (under the right circumstances) undergoes Rabi oscillations where the transition probability is given by equation (2.22)

$$P_E = \sin^2 \left(\frac{\Omega}{2} t \right) \quad (4.2)$$

At the end of that chapter we described Bragg scattering as an effective two level system coupled by a two photon transition and showed that this system undergoes Rabi oscillations with an effective Rabi frequency of (equation (2.105))

$$\Omega_{\text{eff}} = \frac{\Omega}{2\delta} \quad (4.3)$$

¹In principle using this method one can calculate the real atom number but one has to insert the correct dimensions. Since we are only interested in the relative number of atoms that diffracts that is not necessary in our case.

CHAPTER 4. RESULTS

where Ω is the single photon Rabi frequency of the two level atom given in equation (2.12). The Rabi oscillations would be the first prove that we are in the Bragg diffraction regime and would allow us to characterize the setup.

These Rabi oscillations were measured for an intensity of 14 mW, a detuning, δ , from atomic resonance of 2.56 GHz and a frequency shift of 15 kHz between the two Bragg beams. The result of this measurement is plotted in figure 4.2a. The blue data points representing the transition probability (relative number of diffracted atoms) are measured as a function of pulse duration. The dashed orange curve is a fit of a damped sinus which only serves to extract the period of the oscillation. We can now compare the observed period of the Rabi-oscillations with the period that we expect form our calculation for these parameters:

$$\begin{aligned}\text{Calculated period} &= 253.9 \mu\text{s} \\ \text{Measured period} &= 287.9 \mu\text{s}\end{aligned}$$

This shows that there is a small discrepancy between our measurement and our theoretical prediction and they seem to be in very good agreement. The biggest uncertainty in our theoretical calculations is the intensity on the atoms. Due to reflections on the mirrors of the vacuum chamber and diffraction on the atom-chip it is hard to predict what the light field below the chip actually look like. Also, the discrepancy between the two values could be due to the limitations of our theory such as the fact that we only consider a two level atom.

The next feature that one notices in the graph of figure 4.2a is the fact that even in the first oscillation cycle we do not diffract 100 % of the atoms. The maximum diffraction probability is around 80 % which is still not so bad² but higher efficiencies have been achieved. One possible explanation for this observation is the simple fact that we did not optimize our setup. Due to the time pressure after changing the atom chip we simply installed all the optics and when we saw that we diffracted atoms we immediately started measuring without further adjustments. This means that this experiment can simply be improved by adjusting the alignment of the beams and the power balance between the beams. One other likely candidate for the low diffraction amplitude is the distorted wave fronts of the Bragg beams. Because the atoms are very close to the chip the chip is in the way of the beams. This means that they are cut on the chip and interferences below the chip may play a role. In order to reach maximum diffraction the wave fronts of the beams would have to be perfect. Another reason might be that there is besides the condensate still a quite large thermal component which is left behind. The velocity distribution of the thermal component is much larger and might be out of resonance with our Bragg pulse. One more reason for the low diffraction amplitude is related to another feature in the graph. It seems that the oscillation is damped which might already have set in in the first oscillation cycle. The damping of the oscillation is most likely due to the momentum selectivity of the process (see also section 4.4). The damping of the oscillation might also be due to loss of coherence in the condensate but this unlikely since this should take tens of milli seconds.

A second feature of the Rabi oscillation as which we have shown in chapter 3 is that the oscillation period depends on the intensity of light that interacts with the atoms. In fact the frequency of the oscillation is directly proportional to the intensity "seen" by the atoms

$$\Omega_{\text{eff}} \propto I \tag{4.4}$$

This means that if we decrease the intensity the oscillation period should increase. In figure 4.2b we measured this dependence of the oscillation period on the light intensity. The blue data points are measured for a total intensity of 14 mW and the red data points are measured for a total intensity of 7.2 mW. This decrease of power by a factor 2 should increase the oscillation period by the same factor.

²In Bragg scattering light in an AOM the maximum diffraction efficiency is around 85 %

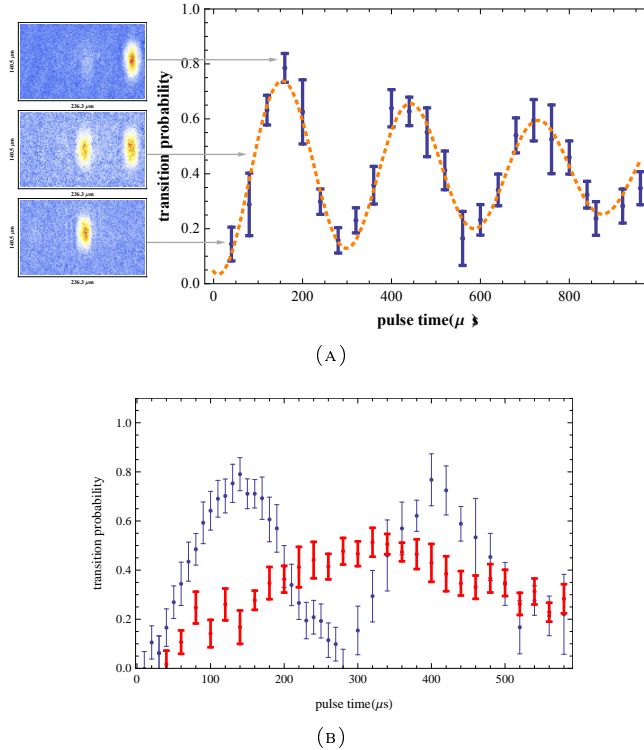


FIGURE 4.2. (A) Measurements of the Rabi oscillation given by the blue data points. The orange curve on is a fit of a damped sinus to extract the oscillation period. The figures on the left serve as an illustration for what figures look like that accompany the data points. This measurement was done for an intensity of 14 mW and a detuning of $\delta = 2.56$ GHz.

(B) Two measurements of the Rabi oscillation for 14 mW(blue curve) and 7.2 mW(red curve). The oscillation period decreases as a function of intensity in the Bragg beams.

Indeed we see that the oscillation period of the red data points is longer than for the blue data points. The fact that for the red data points less atoms get diffracted may be due to the fact that for lower powers the diffraction process becomes more momentum selective. The fact that the red data points are fluctuating more might be caused by a slight imbalance in the power of the Bragg beams which we only became aware of after the measurement.

4.3. Bragg-spectrum

In section 2.6.1 we showed that frequency shift between the two Bragg beams has to satisfy the so called Bragg condition given by equation (2.104) (assuming 0 momentum of the atoms)

$$\delta_n = \frac{(nP_{\text{recoil}})^2}{\hbar 2M} = 15 \text{ kHz} \quad (4.5)$$

where δ_n is the frequency shift between the Bragg beams, M the atomic mass and P_{recoil} the recoil momentum. The Rabi-oscillations that were measured in the previous section were measured assuming this condition. However, in section 3.2.2 we saw that the maximum diffraction amplitude and oscillation period depends on the detuning, δ , from this Bragg resonance. The dependence of the transition probability on the frequency shift between the two Bragg beams is easily calculated and shown in figure 4.3a. We see that, in what we will call the Bragg spectrum, the transition probability has a

sharp peak at the resonance condition of 15 kHz and that it goes down as the frequency shift goes to 0 kHz. The difference in this graph between the blue and the red curve is the intensity of the light. For the simulation of the red curve the power is twice as low as for the blue curve. We see here again the relation that for lower powers the oscillation period goes up which results in a more narrow peak in the Bragg spectrum³.

We measured this Bragg spectrum and the result is shown in figure 4.3b by the blue data points. This measurement was done for a π -pulse of $140\ \mu\text{s}$ determined by the result of the Rabi-oscillation in the previous section and an intensity of 14 mW. In this graph we clearly see the two resonance peaks at -15 and 15 kHz and that for frequency shifts around 0 kHz the diffraction amplitude is close to zero.

Again we notice, as in the Rabi-oscillation, that the maximum diffraction amplitude is about 80 %. This eliminates the possibility that we measured the Rabi-oscillations detuned from resonance. We also see some bumps at the bottom on the inner sides of the diffraction peaks which might be signs of the first reflections. These are the small peaks on the side of the resonance peak in figure 4.3a.

The red data points in figure 4.3b are essentially the same measurement only for a lower light intensity (7.2 mW) and for a more narrow range of frequency shifts. This measurement was done test if the width of the resonance peak becomes more narrow for lower light intensity. On first sight this seems to be the case however, this graph is mildly misleading because the maximum diffraction amplitude is lower for this intensity.

One obvious improvement for this measurement would be to measure with a smaller step size to better resolve the resonance peaks and perhaps the first reflections. Another interesting feature to measure would be to increase the frequency shift to 40 or 50 kHz to try and resolve the second order diffraction. We have tried this very shortly in our experiment without success. However, since the experiment is far from optimized (see section 4.2) this might be possible to observe with the proper adjustments. Also one might observe the higher order diffraction peaks by increasing power but one has to be careful to stay in the Bragg regime.

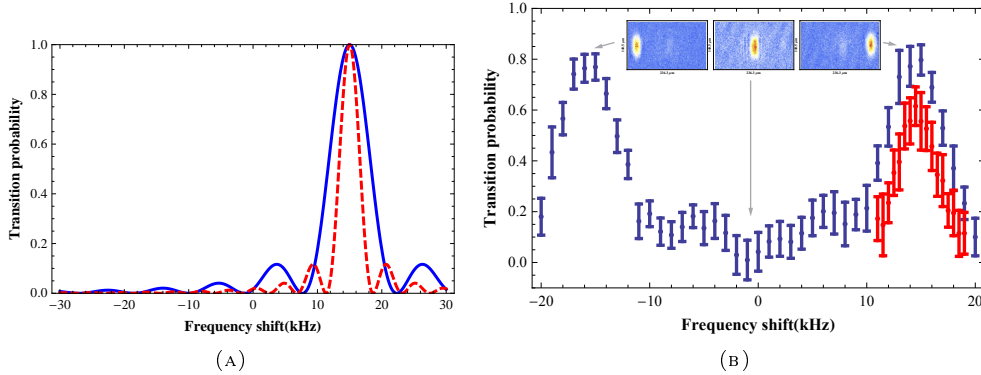


FIGURE 4.3. (A) Calculation of the transition probability as a function of the frequency shift, δ_n , between the Bragg beams. The difference between the blue and red curve is the intensity of the light. For lower intensities (red) we see that the Bragg scattering process becomes more selective. (B) Measurement of the Bragg spectrum. We clearly see that we have a resonant process indicated by the two peaks at -15 kHz and 15 kHz frequency shift. The red data point are the measured for a lower intensity. Unfortunately these measurements are difficult to compare due to the lower diffraction efficiency for lower power.

In figure 4.4 we see the same measurement as in figure 4.3b. The orange curve in this figure is a fit with non adjustable parameters. We determined all the settings of the experiment such as power,

³The width of the peak is effectively given by $\frac{1}{\text{period}}$.

detuning and beams width and used our theoretical model to calculate the spectrum for this setting. We immediately notice one problem with our model which is that it does not take into account the minus first order diffraction. However, the observed width of the resonance peak seems to coincide reasonably well with our calculation.

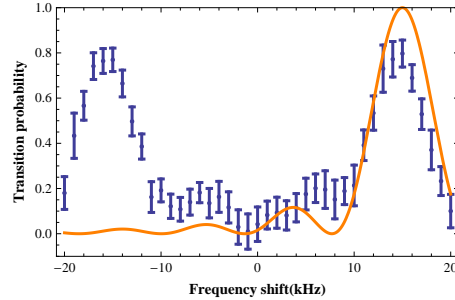


FIGURE 4.4. Measurement of the Bragg spectrum (blue points) and a fit with non adjustable parameters (orange curve). Although the model is not perfect we do see that the observed width coincides quite reasonably with the theoretical model.

4.4. Momentum selectivity

Thus far we have seen two characteristic features of Bragg diffraction. We measured the predicted Rabi oscillations and showed that it is a resonant process. One last feature of Bragg scattering that we encountered in section 2.6.1 is the fact that the Bragg scattering process is momentum selective. This became apparent in equation (2.104) repeated here for the first order

$$\hbar\delta_n = \frac{(P_{\text{recoil}})^2}{2M} + \frac{\mathbf{P}_{\text{atom}} \cdot \mathbf{P}_{\text{recoil}}}{M} \quad (4.6)$$

This equation shows that the resonance condition is dependent on the momentum of the atom. So if we scan the frequency shift between the two Bragg beams we should become resonant with different momentum classes of the momentum distribution. Until this point however, we neglected this second term because the momentum distribution in a Bose-Einstein condensate is very small and around zero momentum. In order to measure this momentum selectivity the momentum distribution has to be larger than the width of the transition. This is illustrated in figure 4.5. The dashed curves represent Bragg pulses with a certain width. If the width of the momentum distribution is more narrow than the width of the Bragg pulse which is the case for a BEC the momentum selectivity can not be resolved⁴. This is illustrated by the purple graph in figure 4.5. If the width of the momentum spread is wider one can diffract atoms depending on their momentum, this case illustrated by the broad blue curve.

To show that Bragg scattering is momentum selective we increased the momentum spread of our sample by raising cut off frequency in our evaporative cooling sequence. This way the atoms do not Bose condense and stay a thermal. We can now do the experiment on a thermal cloud of atoms instead of on a Bose-Einstein condensate⁵.

The results of this measurement are shown in figure 4.6. In seven steps we scanned the frequency shift, δ_n , between the two Bragg beams from 3 kHz to 21 kHz for a pulse of 140 μ s and 14 mW of light intensity. In the picture on the top we see the measurement for a frequency shift of 3 kHz. Here we

⁴This is not necessarily always the case. Moreover one can probe the momentum distribution by giving the Bragg pulse while the BEC is still in the magnetic trap. Then the pulses can be arbitrarily long increasing the momentum selectivity and resolving the momentum distribution of the BEC.

⁵There is an issue here, in order to resolve this process the momentum distribution has to be smaller than the $2\hbar k$ momentum that the atoms get when they are diffracted. In rubidium this point is already very close to condensation.

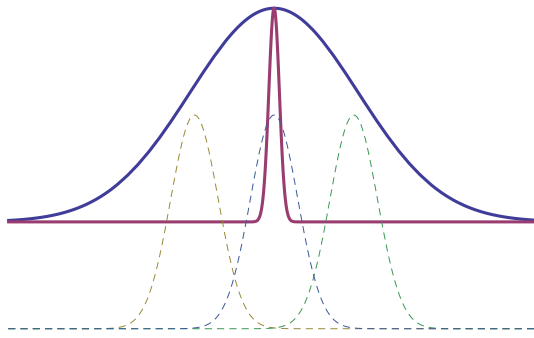


FIGURE 4.5. Illustration of the momentum spread of a BEC (purple curve) and of a thermal cloud (blue curve). In order to resolve the momentum selectivity the momentum spread of the cloud has to be larger than the width of diffraction pulse, indicated by the dashed curves. This is the reason that this experiment was carried out with a thermal cloud.

see that no clear atoms that are diffracted. The not perfect Gaussian shape of the profile might be due to the fact that some atoms are condensed and accumulate in the center. Also the momentum distribution of the a thermal cloud near condensation has a peak around zero momentum [3]. If we look at the figures beneath the top figure we see that for increasing frequency shift atoms from different parts of the cloud start to diffract. The place where the atoms get diffracted is indicated by a red arrow and the place where they get diffracted to is indicated by the green arrow. We observe that as the frequency shift increases the position of the atoms that are diffracted shifts from the left part of the cloud to the right. This shows that as we increase the frequency shift between the Bragg beams we become resonant with atoms with different momentum⁶.

4.4.1. A neat application. One very simple but neat application of the Bragg diffraction is to separate a BEC from its thermal cloud. When a gas of atoms Bose condenses a fraction of the atoms remains thermal. In figure 4.7 we show a qualitative measurement of this application by giving a π -pulse of $140\ \mu\text{s}$ and $14\ \text{mW}$ (-1^{st} order). In the top picture in figure 4.7 we see that the BEC is diffracted to the left and that there remains a cloud of atoms in the original position. If we now look at the profile, the bottom picture in figure 4.7 we see the sharp high peak of the BEC on the left and the broad profile of the remaining thermal cloud on the right. This trick can for example be useful to repeat the measurement of the Rabi oscillation and Bragg spectrum to investigate if higher diffraction amplitudes can be reached.

4.5. Raman-Nath scattering

The results thus far have shown that we can test all the characteristics of Bragg scattering. However, as was mentioned in the introduction of this thesis the aim of the project was to build a versatile experimental setup that can be used for doing many different experiments. The final result that is presented is to show that we can enter a different scattering regime besides Bragg scattering which is called Raman-Nath scattering [21, 22]. The difference between the Bragg and the Raman-Nath regime is that in the Bragg regime the waves scatter from all layers of the diffraction plane add constructively in a single order of diffraction. This happens at the Bragg condition and if the interaction time with the grating is long enough i.e. if it is a thick grating. If the interaction time with the grating is short enough (kinetic energy can be neglected) the diffraction produces a few orders at those angles where

⁶This is true since we do time of flight absorption imaging.

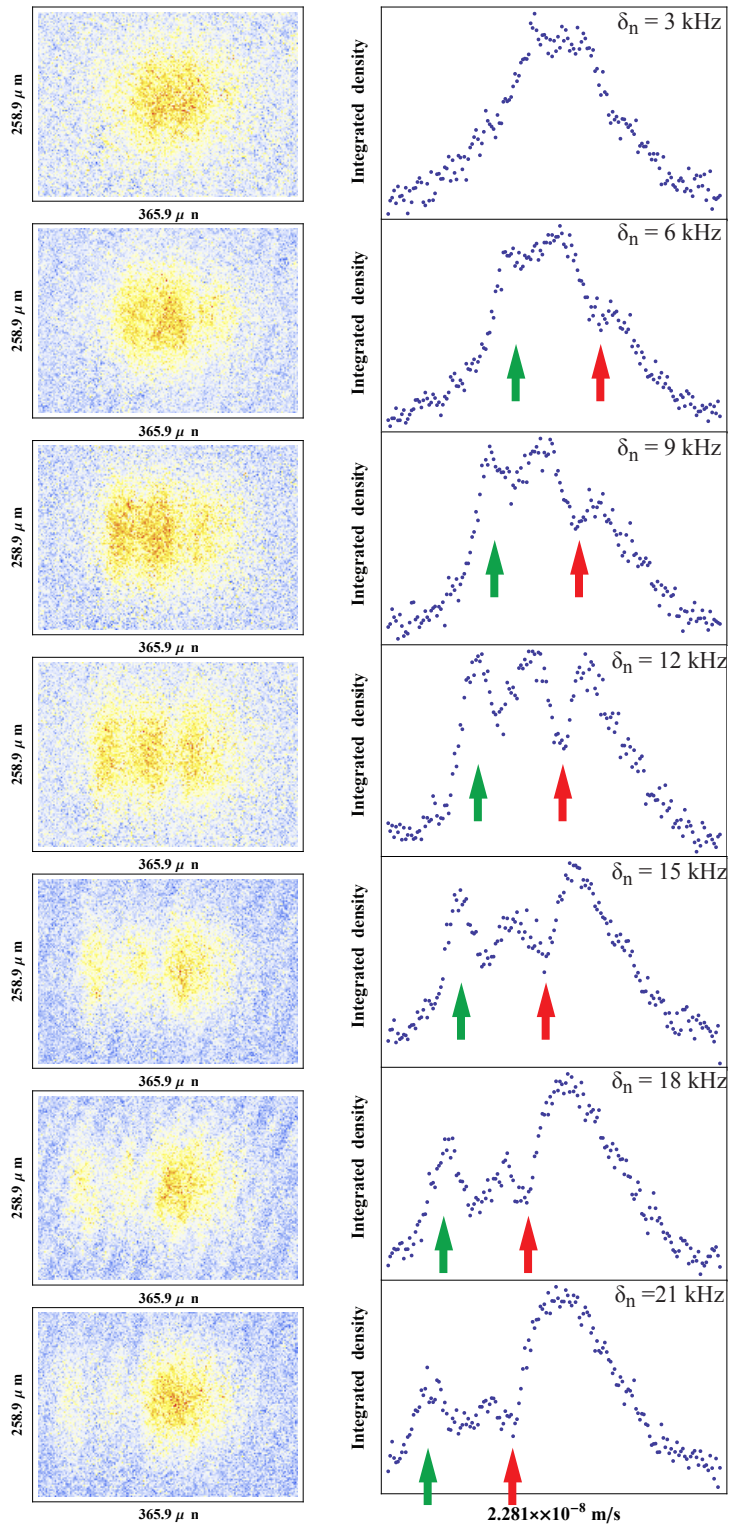


FIGURE 4.6. Measurement of the momentum selectivity of the Bragg scattering process. The frequency shift is scanned from 3 in the top figure to 21 kHz in the bottom figure. We see that the diffracted atoms indicated by the red arrow get scattered to the left indicated by the right arrow. The "diffraction dimple" and diffraction peak shift to the left as the frequency shift increases showing that the pulse becomes resonant with atoms with a different momentum. This demonstrates that Bragg scattering is a momentum selective process.

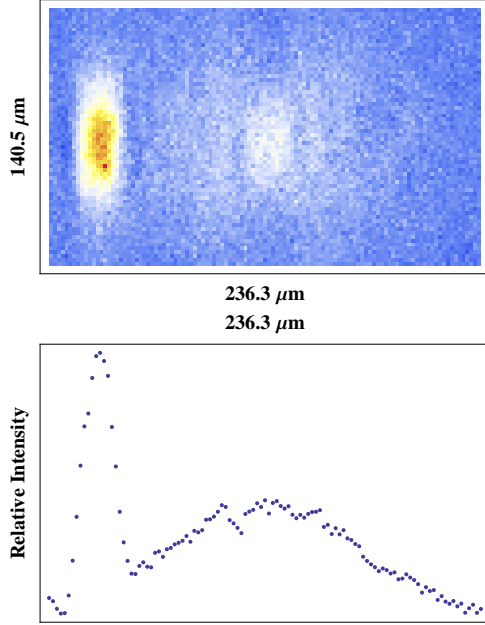


FIGURE 4.7. Above: absorption image of a BEC separated from its thermal cloud (-1^{st} order). Below: profile of the absorption image above. On the left we see the sharp peak of the BEC and on the right you see the broad peak caused by the atoms of the thermal cloud.

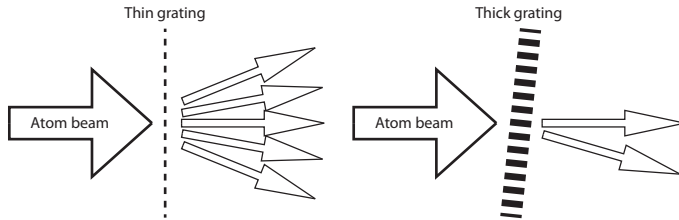


FIGURE 4.8. Difference between scattering of a thin and thick grating. Scattering of a thin grating results in scattering into many order. Scattering of a thick grating if the Bragg condition is satisfied results in scattering into one specific order.

the scatter from all of the grating adds coherently [27]. This "thin" versus "thick" grating scattering is depicted in figure⁷ 4.8 [21].

In figure 4.9 we show the result of giving a pulse of $20\ \mu s$ at an intensity of 41 mW and a frequency shift, δ_n , of 0 kHz thus comprising a standing wave. We clearly see that there are three diffraction peaks, the -1 , 0 and 1 order respectively. This is also reflected in the three sharp peaks of the profile depicted in the lower picture of figure 4.9. This shows that we in this case we diffracted atoms off a standing wave instead off a moving wave (Bragg). Although this is just an qualitative result it does show that the setup can be used to do different experiments than just Bragg. The next step in this case would be to turn on the optical lattice potential adiabatically while the atoms are still in the magnetic trap and to see if we can trap the atoms in the optical lattice. However, this is not directly trivial with this setup since we would need to increase either power or focus the beam which is not

⁷Another way to look at it is that the Fourier spectrum is broader than $4\hbar k$ so that it covers the 1^{st} and -1^{st} order and therefore it is not necessary to be resonant with anything.

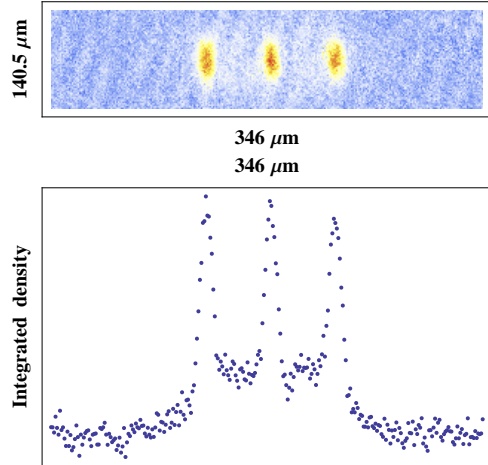


FIGURE 4.9. Top: absorption image of diffraction into many orders at the same time. Instead of diffracting atoms resonantly into either the 1st or -1st order atoms are diffracted into both all orders. This image was taken for a pulse of 20 μ s and 41 mW of light intensity. Below: the vertical profile of the absorption image. We clearly see three peaks. In the center the atoms that did not diffract and on the sides we see the plus and minus first order diffractions. This type of scattering is similar to scattering light of a thin grating.

considering the position of the BEC below the chip. Also the detuning would have to be larger, on the order of several nano meter.

CHAPTER 5

Conclusion & Outlook

The aim of this project was to enhance the atom-chip experiment at the University of Amsterdam with an one-dimensional optical lattice and do Bragg diffraction experiments to characterize this setup. With this setup we observed Rabi oscillations, the Bragg spectrum and momentum selectivity which are the characteristics of the Bragg diffraction.

In this thesis we described the Bragg diffraction as a two-photon transition driving an effective two-level system. In this description we predicted the behavior of the diffraction such as Rabi-oscillations, the Bragg spectrum and the momentum selectivity of this process. To measure these characteristics we have built a laser setup that allows us to control the light intensity of the optical lattice, the detuning from atomic resonance (δ), the pulse duration (τ) and the frequency shift (δ_n) between the two counter propagating beams. Using this setup we observed the Rabi oscillations, the Bragg spectrum and the momentum selectivity and were able to compare our observations with the theoretical model. We can conclude that the observed phenomena are explained well by the theory and we are therefore convinced that we superimposed an optical lattice on the atom-chip experiment.

This was the first goal of this project. The second aim of the project was to build the setup such that there would be enough control over the parameters that is could be used for other experiments than Bragg diffraction. In this thesis we presented one measurement were we showed that with this setup experiments can be done in the Raman-Nath regime by doing short but intense pulses. This observation shows that we are not limited to one case and opens the doors to many more interesting experiments.

The results thus far can be improved by optimizing the setup and doing experiments with a pure BEC for example by first splitting the BEC from the thermal background. It would also be interesting to observe the Rabi-oscillations for a longer time period to observe the overall envelope of the oscillation. Also, if the conditions are improved, it would be nice to observe higher order Bragg diffraction and extend the Bragg spectrum to a wider range of frequency shifts.

Besides optimizing the results that were obtained there are also many possibilities to do new experiments. One option would be to probe the momentum distribution of the condensate by using lower powers (increased momentum selectivity) and long time of flight. Another interesting experiment would be to test Newtons quantum cradle in a single one dimensional condensate. By giving a $\pi/2$ -pulse when the atoms are still in the magnetic trap a part of the atoms start to oscillate in the trap while the other half remains still. By varying the holding time in the magnetic trap one can observe how the atoms thermalize. Yet another experiment that could be done using the Bragg diffraction is atom interferometry. By giving two $\pi/2$ -pulses subsequently one can let two condensates collide and observe atom interference.

Besides the experiments that rely on the Bragg diffraction this laser system might be used as a lattice potential. An experiment that would use the setup as an optical lattice is to increase the intensity of the light (or focus the beam) and increase the detuning and turn on the lattice adiabatically when the atoms are still in the magnetic trap. In this way the atoms could be loaded into the individual traps of the optical lattice. With this setup the Mott-insulator to superfluid transition can be studied in single-sample one-dimensional condensates. To extend the existing setup to this experiment might

still hold some challenges. It is not easy to reach very large detuning with a grating-stabilized diode laser and the position of the BEC directly below the atom chip poses some challenges if one wants to use a focused beam. If this succeeds, science with a BEC in a single array of micro-traps may be used for quantum information. .

APPENDIX A

Fundamental constants

TABLE A.1. Natural constants and rubidium 87 properties used in this thesis

Velocity of light in free space	c	$2.9979 \times 10^8 \text{ m} \cdot \text{s}^{-1}$
Quantum of charge	e	$1.6022 \times 10^{-19} \text{ C}$
Planck's constant	h	$6.626 \times 10^{-34} \text{ J} \cdot \text{s}$
Reduced Plank's constant	$\frac{h}{2\pi}$	$1.0546 \times 10^{-34} \text{ J} \cdot \text{s}$
Boltzmann's constant	k_B	$1.3807 \times 10^{-23} \text{ J} \cdot \text{K}^{-1}$
Electric permittivity of free space	ϵ_0	$8.854 \times 10^{-12} \text{ F} \cdot \text{m}^{-1}$
Magnetic permeability of free space	μ_0	$4\pi \times 10^{-7} \text{ H} \cdot \text{m}^{-1}$
Atomic mass of rubidium	M	$1.443160 \cdot 10^{-25} \text{ kg}$
Effective far-detuned rubidium 87 dipole matrix element	μ	$2.06936 \cdot 10^{-29} \text{ C} \cdot \text{m}$
Rubidium 87 $5^2S_{1/2} \rightarrow 5^2P_{3/2}$ transition wavelength	λ_{D2}	780.241209 nm

APPENDIX B

Saturation intensity

Starting from the optical Bloch equations (2.48a) to (2.48d) we look for the steady state solutions which can be found by setting the time derivatives to zero and using the fact that the total population is conserved and that ρ_{EG} and ρ_{GE} are complex conjugates. We can write the optical Bloch equations including spontaneous emission as

$$\dot{U} = \delta V - \frac{\Gamma}{2} U \quad (\text{B.1a})$$

$$\dot{V} = -\delta U + \Omega W - \frac{\Gamma}{2} V \quad (\text{B.1b})$$

$$\dot{W} = -\Omega V - \Gamma (W - 1) \quad (\text{B.1c})$$

From these equations we immediately see that if $\Omega = 0$ the population difference $W \rightarrow 1$. The steady state solutions are established at times which are long compared to the lifetime of the upper level $t \gg \Gamma^{-1} = \tau$. The resulting equations can be solved for W and give

$$W = \frac{\delta^2 + \Gamma^2/4}{\delta^2 + \Omega^2/2 + \Gamma^2/2} \quad (\text{B.2})$$

This equation we can write in the form

$$W = \left(\frac{2\delta^2}{\Omega^2} + \frac{\Gamma^2}{2} \right) \left(\frac{1}{1 + \frac{2\delta^2}{\Omega^2} + \frac{\Gamma^2}{2}} \right) \quad (\text{B.3})$$

We now define the *saturation parameter* s to be

$$s \equiv \frac{\Omega^2}{2|\Gamma/2 - i\delta|^2} = \frac{\Omega^2}{\Gamma^2/2 + 2\delta} \equiv \frac{s_0}{1 + 4\delta^2/\Gamma^2} \quad (\text{B.4})$$

where in the last step s_0 is the on resonance saturation parameter defined by

$$s_0 \equiv \frac{2\Omega^2}{\Gamma^2} = \frac{I}{I_S} \quad (\text{B.5})$$

with I_S is the saturation intensity given by

$$I_S \equiv \frac{\pi hc}{3\lambda^3\tau} \quad (\text{B.6})$$

These formulas can intuitively be explained by looking at the populations W which can now be written as

$$W = \frac{1}{1+s} \quad (\text{B.7})$$

For a low saturation parameter $s \ll 1$, $W = 1$ and the population is for the larger part in the ground state. For $s \gg 1$ the population is distributed between the excited and ground state ($W = 0$). Using the conservation of population, or $\rho_{EE} + \rho_{GG} = 1$ we can write the population in the upper level as

$$W = 1 - 2\rho_{EE} \Rightarrow \rho_{EE} = \frac{1}{2}(1-W) = \frac{s}{2(1+s)} = \frac{s_0/2}{1+s_0+(2\delta/\Gamma)^2} \quad (\text{B.8})$$

This means that for $s \gg 1$ the population in the excited state tends to $1/2$.

APPENDIX C

Light shift

Besides the effect on the populations radiation that perturbs the atoms also changes the energy level of the atoms. It is possible to treat the effect of far-detained laser light on the atomic energy levels as a second order perturbation of the electric field, i.e. linear in terms of the field intensity [15]. The energy shift given by second-order time-independent perturbation theory is given by

$$\Delta\mathcal{E}_i = \sum_{j \neq i} \frac{|\langle j | \mathcal{H} | i \rangle|^2}{\mathcal{E}_i - \mathcal{E}_j} \quad (\text{C.1})$$

For an atom interacting with a laser field the perturbing Hamiltonian is given by equation (2.8). To determine the relevant energies E_i and E_j we have to consider the combined system of atom plus the radiation field, this is called the *dressed state* view and was first introduced by Cohen-Tannoudji in 1992 [15]. If the atom is in the ground state it has zero internal energy and all the energy is in the radiation field. For a field consisting of n photons this is given by $n\hbar\omega$. If an atom absorbs an photon from the radiation field it gains internal energy of $\hbar\omega_0$ whereas the laser field loses an photon of energy $\hbar\omega$ leaving $(n - 1)\hbar\omega$. Now considering our two level atom with only ground and excited state equation (C.1) becomes

$$\Delta\mathcal{E}_G = \sum_{E \neq G} \frac{|\langle E | e\mathbf{r} \cdot \mathbf{E} | G \rangle|^2}{\mathcal{E}_G - \mathcal{E}_E} = \frac{|\langle E | e\mathbf{r} \cdot \mathbf{E}_0 | G \rangle|^2}{4\hbar\delta}$$

The same can be done for the excited state. We can now use definition (2.12) to replace transition matrix element to obtain

$$\Delta\mathcal{E} = \pm \frac{\hbar\Omega^2}{4\delta}$$

This we can rewrite in terms of the light field intensity using equation (B.5) which will give

$$\Delta\mathcal{E} = \pm \frac{\hbar}{4\delta} \frac{\Gamma^2 I}{2I_s}$$

Replacing the saturation intensity by equation (B.6) we get

$$\begin{aligned} \Delta\mathcal{E} &= \pm \frac{\hbar}{4\delta} \frac{\Gamma^2 I}{2} \frac{3\lambda^3 \tau}{\pi hc} \\ &= \pm \frac{3c^2 \pi \Gamma I}{2\omega_0^3 \delta} \end{aligned}$$

This perturbative result obtained for the energy shifts is exactly the same as the dipole potential for the two-level atom given in equation (2.82). This light induced energy shift is also referred to as the ac-Stark shift. If we consider low intensities in which case the atom will spend most of its time in the ground state one can interpret the light shifted ground state as the relevant potential for the motion of atoms (figure)[15].

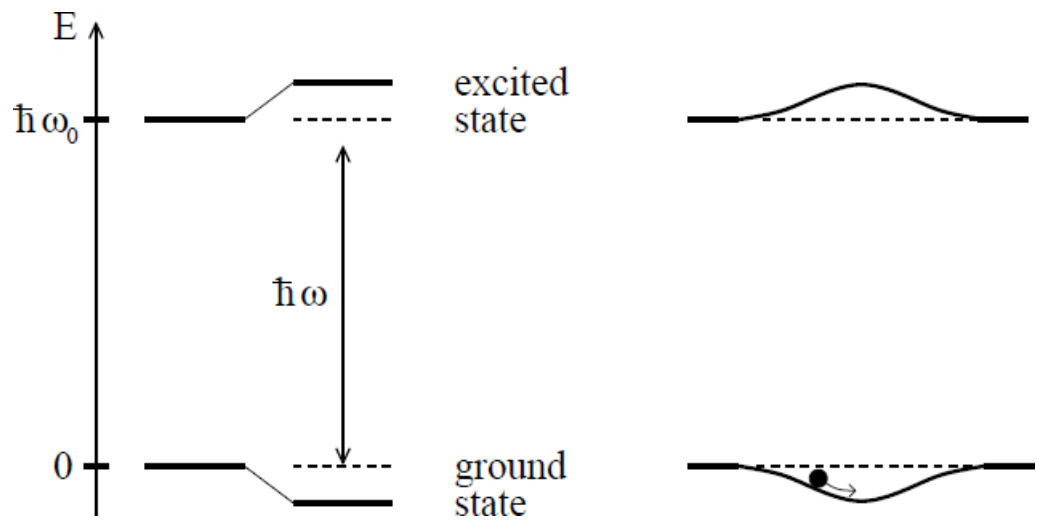


FIGURE C.1. The light shift for a two-level atom. The left picture indicates the light shift for red detuned light. The ground state is shifted down whereas the excited state is shifted up. On the right picture, an inhomogeneous light field such as an Gaussian laser beam produces a ground state potential well which can be used to trap atoms. Picture taken from [15].

APPENDIX D

Radiative selection rules

For optical transitions the coupling between atomic states is given by the dipole moment, and selection rules exist for such transitions [11]. In reality the atomic structure is considerably more complicated than the two-level atom model discussed in most of chapter 2. These selection rules are calculated in most quantum mechanics textbooks such as [28] and will not be calculated here. In this appendix we want to point out one important situation in which atoms with angular-momentum degeneracy behave as two-level atoms. This is situation in which a transition of the form $F \rightarrow F' = F + 1$ is pumped by circulary polarized light. Consider the $F_G = 1 \rightarrow F_E = 2$ transition coupled by σ_+ -polarized light. This transition drives sublevel transitions of the form $M_F \rightarrow M'_F = M_F + 1$. However the spontaneous emission from M'_F occurs via $M'_F \rightarrow M_F = M'_F \pm 0, 1$ [29]. This gives rise to the scheme depicted in figure D.1. In this figure we see that the $F = 1, M_F = 1 \rightarrow F' = 2, M'_F = 2$ transition is a closed scheme. All atoms that start out in any other state than this are optically pumped into this cycling transition. In steady state we effectively have an two level atom (figure D.2).

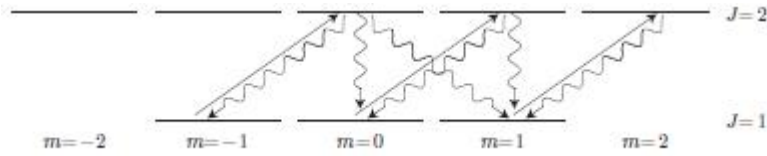


FIGURE D.1. Optical transitions of the form $F \rightarrow F + 1$ which is pumped by σ_+ -circulary polarized light.

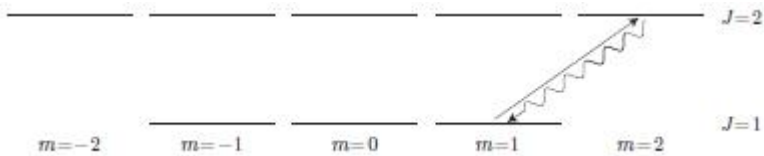


FIGURE D.2. Optically pumping the $F \rightarrow F' = F + 1$ transition with σ_+ -circulary polarized light will result in an effective two-level atom cycling transition.

APPENDIX E

Effective Rabi-frequency for first order Bragg scattering

Bragg diffraction of a collimated atomic beam by a standing wave can be thought of scattering the atomic deBroglie waves from the dipole potential of the atom-light interaction. To understand the process of Bragg scattering the key is to recognize that in Bragg scattering the initial and final momentum states we encountered in the previous section are resonantly coupled through a multiphoton process. So we can treat this problem very similar to how we treated the Rabi two-level problem in section 2.1 [23]. A transition between two states that involves two photon absorptions from two different laser beams is also called a Raman transition. By adapting the single photon treatment of the two-level problem we will try to get a physical insight into Raman transitions. The same results can be achieved more rigorous by second-order time-dependent perturbation theory but this approach will give a more physical insight [10]. A Raman transition involves two laser beams with frequencies ω_{L1} and ω_{L2} respectively. The atom interacts with the electric field which now has two frequency components, $\mathbf{E} = \mathbf{E}_{L1} \cos(\omega_{L1}) + \mathbf{E}_{L2} \cos(\omega_{L2})$. In our case we will look at a transition between two momentum states of the ground state of an atom (figure E.1). This treatment involves a virtual energy level $|i\rangle$ which stands for intermediate but to which atoms are not actually excited. This means that this treatment is not comprised of two single photon processes, $|G, 0\rangle \rightarrow |i\rangle$ followed by $|i\rangle \rightarrow |G, 2\hbar k\rangle$, but happens instantaneously [10]. The energy diagram for this transition is shown in figure E.1.

Let us start by only consider the perturbation of the atom by light with frequency ω_{L1} . For this situation exactly the same equations as given in section 2.1 up to equation (2.14b) are valid. However we are now perturbing our atom with light of frequency ω_{L1} instead of light with frequency ω . So the detuning from atomic resonance now becomes $\delta \equiv \omega_{L1} - \omega_0$ ¹. With this definition we get

¹The use of δ 's throughout this thesis might become confusing. In this case nothing has changed compared to section (2.1) and δ is still the detuning from atomic resonance only now with ω_{L1} instead of ω . Also for further reference δ without any subscript or indication always refers to the detuning from atomic resonance. If it has any other meaning this is indicated via a subscript or index.

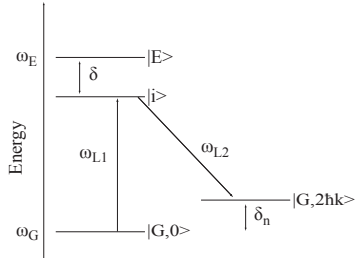


FIGURE E.1. Energy schematic of the 2-photon transition. An atom in the $|G, 0\rangle$ state absorbs a photon with frequency ω_{L1} and is excited to a imaginary energy level $|i\rangle$. The atom is then stimulated to emit a photon with frequency ω_{L2} to end up in the "excited state" $|G, 2\hbar k\rangle$. Detuning from atomic resonance has to be large to prevent real excitations and the detuning between the two laser beams has to be on "Bragg resonance".

$$c_E(t) = -\frac{\Omega^*}{2} \left(\frac{1 - e^{-i\delta t}}{\delta} \right) \quad (\text{E.1})$$

Now plugging this result into equation (2.2) to obtain the wavefunction

$$\Psi(\mathbf{r}, t) = e^{-i\omega_G t} |G\rangle - \frac{\Omega^*}{2\delta} e^{-i\omega_E t} |E\rangle + \frac{\Omega^*}{2\delta} e^{-i(\omega_G + \omega_{L1})t} |E\rangle \quad (\text{E.2})$$

$$= e^{-i\omega_G t} |G\rangle - \frac{\Omega^*}{2\delta} e^{-i\omega_E t} |E\rangle + \frac{\Omega^*}{2\delta} e^{-i\omega_i t} |E\rangle \quad (\text{E.3})$$

We see that the perturbation produces an admixture of two terms into the excited state that both have the same (small) amplitude. The first term describes the real excitation to the excited state. The term with angular frequency $\omega_G + \omega_{L1} = \omega_i$ corresponds to the *virtual* level. Mathematically this term acts as if there is an energy level at ω_i that has the same symmetry properties as the excited state. However in reality such an energy level does not exist [10]. So far nothing much has changed compared to what we have seen in section (2.1). The next thing is to determine the effect of the with angular frequency ω_{L2} on the already perturbed atom. We now start from equations (2.11) however we replace $\omega \rightarrow \omega_{L2}$ and the atomic resonance frequency by $\omega_0 \rightarrow \omega_E - \omega_{G,2\hbar k}$. Also since we are looking at an already perturbed atom all the G 's in equations (2.11) are replaced by E and the excited state is now the excited momentum state of the ground state and is written down as $|G, 2\hbar k\rangle$. With these substitutions we find that

$$i\dot{c}_{G,2\hbar k} = c_E e^{i(\omega_E - \omega_{G,2\hbar k})t} \cos(\omega_{L2}t) \Omega^* \quad (\text{E.4})$$

The coefficients c_E was already determined in equation (E.1). which combines to give the following result

$$\begin{aligned} i\dot{c}_{G,2\hbar k} &= -\frac{\Omega^* \Omega^*}{2\delta} \cos(\omega_{L2}t) e^{-i(\omega_E - \omega_{G,2\hbar k})t} (1 - e^{-i\delta t}) \\ \Rightarrow i\dot{c}_{G,2\hbar k} &= -\frac{\Omega^2}{4\delta} (e^{i\omega_{L2}t} + e^{-i\omega_{L2}t}) (e^{-i(\omega_E - \omega_{G,2\hbar k})t} - e^{-i(\delta + \omega'_0)t}) \\ \Rightarrow i\dot{c}_{G,2\hbar k} &= -\frac{\Omega^2}{4\delta} \left(e^{i(\omega_{L2} - \omega_E + \omega_{G,2\hbar k})t} + e^{-i(\omega_{L2} + \omega_E - \omega_{G,2\hbar k})t} \right. \\ &\quad \left. - e^{i(\omega_{L2} - \delta - \omega_E + \omega_{G,2\hbar k})t} - e^{-i(\omega_{L2} + \delta + \omega_E - \omega_{G,2\hbar k})t} \right) \quad (\text{E.5}) \end{aligned}$$

Basically what we have her is the same situation as we encountered before in equation (2.14b). If we now do the same integration with initial condition $c_E(0) = 1$, $c_{G'}(0) = 0$ and immediately apply the rotating wave approximation we are left with

$$c_{G,2\hbar k} = \frac{\Omega^2}{4\delta} \left(\frac{1 - e^{-i(\omega_E - \omega_{G,2\hbar k} - \omega_{L2})t}}{(\omega_E - \omega_{G,2\hbar k} - \omega_{L2})} + \frac{1 - e^{i(-\delta - \omega_E + \omega_{G,2\hbar k} + \omega_{L2})t}}{(-\delta - \omega_E + \omega_{G,2\hbar k} + \omega_{L2})} \right) \quad (\text{E.6})$$

Let us now define the detuning from Bragg resonance. If we look at figure E.1 we see that we can write this down as

$$\delta_{\text{Bragg}} \equiv (\omega_{L1} - \omega_{L2}) - (\omega_{G,2\hbar k} - \omega_G) = \delta_n - (\omega_{G,2\hbar k} - \omega_G) \quad (\text{E.7})$$

which is independent of ω_i . In the case that we have studied here the Raman transition can be viewed as a coupling between the levels $|G, 0\rangle$ and $|G, 2\hbar k\rangle$ via a virtual energy level at ω_i . The next step is to write equation (E.6) in terms of δ_{Raman} which gives the following result

$$c_{G,2\hbar k} = \frac{\Omega^2}{4\delta} \left(\frac{1 - e^{-i(\delta + \delta_{\text{Bragg}})t}}{(\delta + \delta_{\text{Bragg}})} - \frac{1 - e^{-i\delta_{\text{Bragg}}t}}{\delta_{\text{Bragg}}} \right) \quad (\text{E.8})$$

The most interesting case would be to look at situations where the Raman transition is resonant, thus at $\delta_{\text{Bragg}} \simeq 0$ and at large detunings, $\delta \gg \delta_{\text{Raman}}$. This ensures that there is no population in the

excited state and we can forget about spontaneous emission [10]. In this case we can eliminate the first term in equation E.8 and we end up with the following equation

$$c_{G,2\hbar k} = \frac{\Omega^2}{4\delta} \left(\frac{1 - e^{-i\delta_{\text{Bragg}} t}}{\delta_{\text{Bragg}}} \right) \quad (\text{E.9})$$

If one defines an effective Rabi frequency as

$$\Omega_{\text{eff}} \equiv \frac{\Omega^2}{2\delta} \quad (\text{E.10})$$

equation (E.9) becomes

$$c_{G,2\hbar k} = -\frac{\Omega_{\text{eff}}}{2} \left(\frac{1 - e^{-i\delta_{\text{Bragg}} t}}{\delta_{\text{Bragg}}} \right) \quad (\text{E.11})$$

This is exactly the same result as we found in equation (2.15) for single photon excitation only is Ω replaced by Ω_{eff} . This description of Raman transitions has assumed a weak perturbation by the light field analogous to what we found in section 2.1.2.1 for a single photon excitation. A treatment of the system in the same way as in section 2.1.2.2 with Rabi frequency Ω_{eff} will show that this Raman transition will give rise to Rabi oscillations [10]. For example a π -pulse will transfer all the population from one momentum state to the other. This has already been observed experimentally with a stationary sodium BEC in [19].

Bibliography

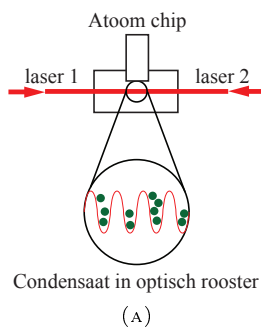
- [1] S. Bose, “Plancks gezets und lichtquantenhypothese,” *Zeitschrift fur physik a hadrons and nuclei*, vol. 26, no. 1, 1924.
- [2] A. Einstein, “Quantentheorie des einatomigen idealen gases,” *Sitzungsberichte der preussischen akademie der wissenschaften*, 1924.
- [3] E. Cornell and C. Wieman, “Bose-einstein condensation in a dilute gas, the first 70 years and some recent experiments,” *International Journal of Modern Physics B*, vol. 16, no. 30, 2002.
- [4] K. Bongs and K. Stengstock, “Physics with coherent matter waves,” *Reports on progress in physics*, vol. 67, no. 6, 2004.
- [5] A. van Amerongen, *One-dimensional bose gas on an atom chip*. PhD thesis, University of Amsterdam, 2008.
- [6] J. van Es, *Bose-Einstein condensates in radio-frequency-dressed potentials on an atom chip*. PhD thesis, University of Amsterdam, 2009.
- [7] T. Kinoshita, T. Wenger, and D. Weiss, “A quantum newtons cradle,” *Nature*, vol. 440, 2006.
- [8] I. Bloch, “Ultracold quantum gases in optical lattices,” *Nature physics*, vol. 1, 2005.
- [9] P. Treutlein, T. Steinmetz, Y. Colombe, B. Lev, P. Hommelhoff, J. Reichel, O. Greiner, M. Mandel, A. Widera, T. Rom, I. Bloch, and T. Hansch, “Quantum information processing in optical lattices an magnetic microtraps,” *Fortschritte der physik*, vol. 54, 2006.
- [10] C. Foot, *Atomic physics*. New York: Oxford University Press, 2005.
- [11] H. Metcalf and P. van der Straten, *Laser cooling and trapping*. Springer, 1999.
- [12] R. Feynman, F. Vernon, and R. Hellwarth, “Geometrical representation of the schrodinger equation for solving master problems,” *Journal of applied physics*, vol. 28, no. 1, 1957.
- [13] W. Phillips, P. Lett, R. Watts, and C. Westbrook, “Observation of atoms laser cooled below the doppler limit,” *Physical Review Letters*, vol. 61, no. 2, 1988.
- [14] J. Dalibard and C. Cohen-Tannoudji, “Laser cooling below the doppler limit using polarization gradients: simple theoretical models,” *Optical society of America*, vol. 6, no. 11, 1989.
- [15] R. Grimm, M. Weidemuller, and Y. Ovchinnikov, “Optical dipole traps for neutral atoms,” *Advances in atomic, molecular and optical physics*, vol. 42, 2000.
- [16] D. Pritchard, “Cooling neutral atoms in a magnetic trap for precision spectroscopy,” *Physical review letters*, vol. 51, no. 15, 1983.
- [17] M. Anderson, M. Ensher, J.R. Matthews, C. Wieman, and E. Cornell, “Observation of bose-einstein condensation in a dilute atomic vapor,” *Science*, vol. 269, no. 5221, 1995.
- [18] K. Davis, M.-O. Mewes, M. Andrews, N. van Druten, D. Durfee, D. Kurn, and W. Ketterle, “Bose-einstein condensation in a gas of sodium atoms,” *Physical review letters*, vol. 75, no. 22, 1995.
- [19] M. Kozuma, L. Deng, E. Hagley, J. Wen, R. Lutwak, K. Helmerson, S. Rolston, and W. Phillips, “Coherent splitting of bose-einstein condensed atoms with optically induced bragg diffraction,” *Physical review letters*, vol. 82, no. 5, 1999.
- [20] J. Denschlag, J. Simsarian, C. Haffner, H. McKinzie, D. Browaeys, A. Cho, K. Helmerson, S. Rolston, and W. Phillips, “A bose-einstein condensate in an optical lattice,” *Journal of physics B: atomic, molecular and optical physics*, vol. 35, 2002.
- [21] A. Cronin, J. Schmiedmayer, and D. Pritchard, “Optics and interferometry with atoms and molecules,” *Reviews of modern physics*, vol. 81, 2009.
- [22] P. Martin, B. Oldaker, A. Miklich, and D. Pritchard, “Bragg scattering of atoms from a standing light wave,” *Physical review letters*, vol. 60, no. 6, 1988.
- [23] D. Giltner, R. McGowen, and S. Lee, “Theoretical and experimental study of the bragg scattering of atoms from a standing light wave,” *Physical review A*, vol. 52, no. 5, 1995.
- [24] M. Greiner, O. Mandel, T. Esslinger, T. Hansch, and I. Bloch, “Quantum phase transition from a superfluid to a mott insulator in a gas of ultracold atoms,” *Nature*, vol. 415, 2002.

-
- [25] J. Stenger, S. Inouye, A. Chikkatur, D. Stamper-Kurn, D. Pritchard, and W. Ketterle, "Bragg spectroscopy of a bose-einstein condensate," *Physical review letters*, vol. 82, no. 23, 1999.
 - [26] D. Smith, S. Aigner, S. Hofferberth, M. Gring, M. Andersson, S. Wildermuth, P. Kruger, S. Schneider, T. Schumm, and J. Schmiedmayer, "Absorption imaging of ultracold atoms on atom chips," *Optical society of America*, vol. 19, no. 9, 2011.
 - [27] H. Muller, S. Chiow, and S. Chu, "Atom-wave diffraction between the raman-nath and the bragg regime: Effective rabi frequency, losses, and phase shifts," *Physical review A*, vol. 77, 2008.
 - [28] C. Cohen-Tannoudji, B. Diu, and F. Laloe, *Quantum mechanics*. Hermann, 2005.
 - [29] D. Steck, "Quantum and atom optics." online publication available at <http://www.opencontent.org/openpub> visited 26-April-2012, 2005.

Nederlandse samenvatting

In 1924 deden de twee natuurkundigen Bose en Einstein een belangrijke voorspelling [1, 2]. Zij voorspelden dat bij hele lage temperaturen, rond de *nano* Kelvin, een gas atomen een speciaal soort fase overgang zou ondergaan. De atomen zouden niet, zoals normaal, een vaste stof worden maar een nieuw soort materie vormen. Deze vorm van materie staat tegenwoordig bekend als het Bose-Einstein condensaat. Het heeft natuurkundigen bijna 70 jaar gekost om deze vorm van materie te maken. Waarom zijn wetenschappers zo gedreven geweest om deze exotische substantie te maken? Het bijzondere aan een Bose-Einstein condensaat is dat bij deze lage temperaturen alle atomen in het laagst mogelijke quantum energie niveau gaan zitten. In deze toestand overlappen de materie golven van de individuele atomen elkaar dusdanig dat ze niet meer te onderscheiden zijn en als het ware een grote materie golf vormen (ook wel superatoom genoemd). Een interessant fenomeen van dit verschijnsel is dat quantum mechanische effecten een rol spelen op een macroscopisch niveau.

Hier op de Universiteit van Amsterdam wordt het onderzoek met Bose-Einstein condensaten niet op de traditionele manier gedaan maar met behulp van *atoom-chips* (figuur B). Met behulp van een atoom-chip kunnen condensaten worden gemaakt die bij benadering een dimensionaal zijn [5]. Tijdens dit onderzoek is dit atoom-chip experiment uitgebreid door een een dimensionale optische rooster potentiaal toe te voegen. Door twee laser bundels in tegengestelde richting te schijnen ontstaat er een staande golf. De atomen in een Bose-Einstein condensaat zijn gevoelig voor de elektromagnetische potentiaal die wordt gecreëerd door de staande golf. Hierdoor ontstaat een *optisch rooster* van maxima en minima dat gebruikt kan worden om de atomen te manipuleren (figuur A).



(A)

Opstelling van de 1-dimensionale rooster potentiaal. De atomen worden onder de atoom-chip gevangen en in een optisch rooster geladen.



(B)

Foto van de atoom-chip. De atoomchip is gemaakt van een dun laagje goud op een silicium basis. Hierop is een patroon van draden gegraveerd dat gebruikt wordt om magnetische velden mee op te wekken om de atomen mee te manipuleren.

Voor dit specifieke onderzoek is een experiment gedaan om aan te tonen dat het condensaat wisselwerking heeft met het optisch rooster. Om dit te laten zien is er gebruik gemaakt van *Bragg*

diffractie. Bragg diffractie lijkt op het experiment waarbij licht op een tralie wordt geschoten, achter het tralie is dan een interferentie patroon waar te nemen. Onder de juiste omstandigheden kan dit experiment zo gedaan worden dat het licht niet verstrooid in veler orders maar slecht in één specifieke orde. Met dit type experiment kan informatie worden verkregen over de tralie en de interactie met het licht. Met een Bose-Einstein condensaat kan een soortgelijk experiment worden gedaan. In dit geval wordt de het tralie vervangen door het optisch rooster en de licht bundel door de materie golf van het Bose-Einstein condensaat.

In dit onderzoek hebben wij kunnen laten zien dat er een grote mate van controle is over onze opstelling en dat de atomen kunnen worden gemanipuleerd op een manier die van te voren is voorspeld. Deze opstelling in combinatie met het 1-dimensionale karakter van de condensaten kunnen in de toekomst gebruikt worden voor veel verschillende en razend interessante experimenten, bijvoorbeeld door de atomen in de individuele vallen van de staande golf te laden.

Acknowledgments

In this final piece I would like to acknowledge all the people who contributed in some way to the realization of this thesis. First of all I want to thank Wojciech Lewoczko-Adamczyk who has been my daily supervisor for the past year. You have always been optimistic even at times when the future seemed dark. You have been a stimulating and inspiring supervisor who showed me a side of science I had not seen before. I really enjoyed working together and hope we get to shake hands again when you return to Amsterdam. Furthermore I would like to thank my supervisor Klaasjan van Druten for always being calm and serene even when the atom-chip exploded. You have always been helpful and your office was always open for questions. I regret that the experimental data came so late in the year. I would like to have had more discussions about the experiment and all the possibilities that exist now. I also wish to thank the other members of the group Quentin Beaufils and Steven Lepoutre. Especially after Wojciech left you always had time to help me out with the experiment and proof reading my thesis. There was always a really relaxed and stimulating ambiance in lab and you were never too busy to help. Then I want to thank all the other members of the quantum gases and quantum information group at the University of Amsterdam. Arteju, Richard, Vanessa and Slava for having time to help me out when I was stuck with Mathematica or when there were problems in the lab. Also thanks to Ben van den Linden van den Heuvell for showing me some useful tricks in Mathematica and for being my second supervisor.

Bij deze wil ik graag ook wat mensen bedanken die niet direct hebben bij gedragen aan de natuurkunde van deze thesis maar zonder wie dit nooit tot stand zou zijn gekomen. Allereerst mijn ouders, niet alleen voor de financiële steun tijdens mijn studie maar vooral ook voor het onvoorwaardelijke vertrouwen en de interesse in mij. Pa, mam bedankt! Daarnaast wil ik graag Nick bedanken voor zowel binnen als buiten de universiteit een goede vriend en altijd zijn relaxte zelf te zijn. Verder wil ik graag Chris en alle overige leden van de hard condensed matter groep bedanken voor de levendige koffie pauzes. Als allerlaatste wil ik Shira bedanken. Ondanks dat wij in een ongebruikelijke situatie verkeerde was jij er altijd voor mij, dankjewel.